AN OPTIMAL APPROACH TO COMPUTER CONTROL OF A HIGHLY COUPLED SATELLITE ATTITUDE LOOP

by

WILLIAM NEIL McCASLAND

B.S., United States Air Force Academy
1979

Submitted in partial fulfillment of the
requirements for the degree of
MASTER OF SCIENCE
at the
Massachusetts Institute of Technology
September 1980

Signature of Author _____
Department of Aeronautics and Astronautics
September 30, 1980

Approved by _____
Kevin C. Daly
Technical Supervisor, CSDL

Certified by _____
Richard H. Battin
Thesis Supervisor

Accepted by _____
Harold Y. Wachman
Chairman, Departmental
Graduate Committee

ABSTRACT

AN OPTIMAL APPROACH TO COMPUTER CONTROL OF A HIGHLY COUPLED SATELLITE ATTITUDE LOOP

by

William Neil McCasland

Submitted to the Department of Aeronautics and Astronautics on September 1980 in partial fulfillment of the requirements for the degree of Master of Science

Linear-Quadratic-Gaussian optimal control theory provides a unified approach to controller synthesis. The pitch and array drive loop of the DMSP Block 5D spacecraft, which represents an interesting control problem because of actuator coupling, is considered as an example. A discrete-time optimal feedback control law timed to match the Block 5D's flight computer is determined. New cross feeds result that are not present in the current control laws, derived by classical compensation, which exploit the array drive motor's reaction torque on the satellite body to enhance body pointing at the expense of array error. Reaction wheel activity can, in certain cases, be reduced by a factor of five.

The requirement of full state knowledge is met by an estimator developed according to discrete time Kalman filtering theory. Several measurement options were considered which included rate integrating gyros as currently exist on the satellite, a 2-D star mapper sensing catalogued stars, and the combination of a star mapper and rate gyro measurements. Although the use of integrating gyros allows extremely accurate short-term attitude estimation, the star mapper concept presented is able to show acceptable accuracy. Coupled with the latter's low relative cost and lack of long-term drift, it appears that a star mapper can be a good alternative inertial sensor.

Closed-loop results, using an estimator driven by star-mapper grade measurements, indicates that the optimal control law is able to meet the tight (0.01°) body pointing specification in the presence of

worst case external and internal disturbance torques. In addition, when compared to the current control law, the optimal controller shows less sensitivity in terms of mean-square pointing error to measurement noise.

Thesis Supervisor: R.H. Battin, Ph.D.

Title: Associate Department Head,
The Charles Stark Draper Laboratory;
Adjunct Professor,
Department of Aeronautics and Astronautics

Thesis Supervisor: K.C. Daly, Ph.D.

Title: Program Director,
The Charles Stark Draper Laboratory

ACKNOWLEDGMENT

This report was prepared at The Charles Stark Draper Laboratory, Inc. under Purchase Order Number 300001-F42 with RCA. The author's graduate studies at the Massachusetts Institute of Technology were supported by the Fannie and John Hertz Foundation.

The author wishes to express his sincere appreciation to Dr. Kevin Daly for his time, patience, and counsel in the preparation of this thesis. Appreciation is also extended to Dr. Richard Battin for his time spent as the MIT faculty supervisor.

The time and effort invested by Dr. Bill Podgorsky in technical support with his knowledge of the Block 5D system was invaluable. Finally, the quality of this document's publication is a result of the publication assistance from Faye Budlong.

TABLE OF CONTENTS

TABLE OF CONTENTS (Cont.)

CHAPTER 1

INTRODUCTION

Attitude control of small satellites, where rigid body dynamics dominate, has become routine engineering practice. Classical frequency domain compensation is a mature body of theory that is well suited for designing such controllers, and is almost universally employed. However, future large space structures, because of the numbers of modes, actuators, and sensors, will present problems that are not approachable with classical theory and will require application of modern optimal control theory characterized by state space modeling. Unfortunately, modern theory does not have the long history of application that frequency domain techniques do. It is useful to consider the application of modern theory to low-order satellite problems where, although classical techniques are proven, the potential for performance enhancement exists. Such applications also stand to clearly illustrate the differences between modern and classical theory and advance the maturity of the former. This thesis will take as an example the Defense Meterological Space Program (DMSP) Block 5D satellite.

The Block 5D, illustrated in Figure 1-1, is an operational earth observation satellite and is launched into sun syncronous near-circular orbits of approximately 450 nmi altitude. A large solar array has a driven rotational degree of freedom along the pitch axis, which significantly affects the satellite's inertial properties.

1.1 Control Objectives

Once nearly nominal attitude is established after launch, the Primary Attitude Determination and Control System (PADACS) assumes

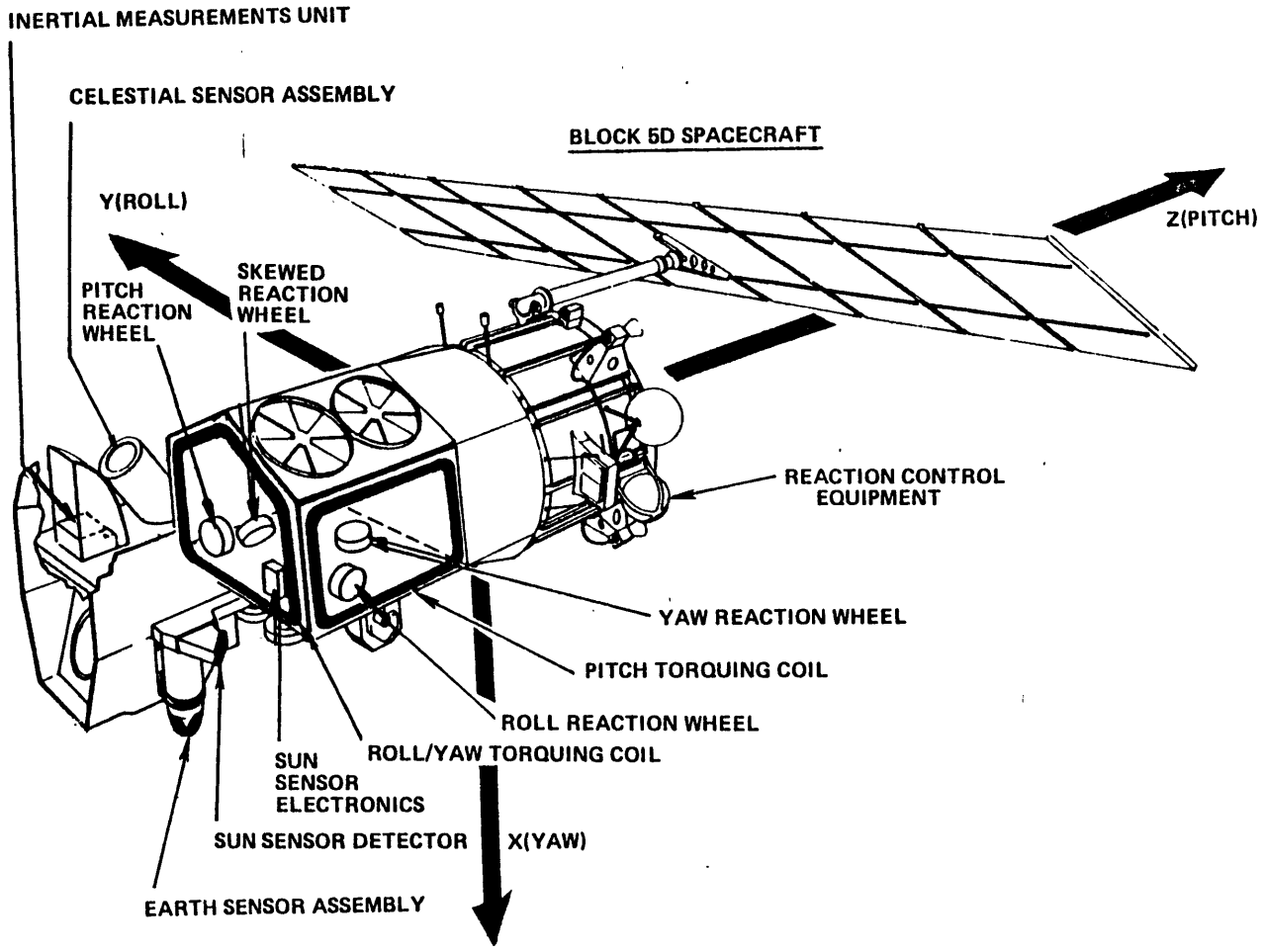

Figure 1-1. Block 5D spacecraft configuration.

command for the remainder of the mission. Since the mission is earth observation, the roll and pitch axes must be maintained in a local-level plane with the roll axis parallel to the velocity vector. To maintain local level, a near steady state pitch rate, nominally 0.06 deg/s, is required. The solar array is to track the sun, and therefore should not rotate with respect to inertial space although it will appear to do so from the satellite.

Specific pointing error limits are

body axes	±0.01 deg
array angle	±3.0 deg

The extremely tight control specification on body pointing is not common with most spacecraft, and coupled with the inertial properties of the B5D, make this a fairly unique problem.

To achieve such a level of precision, the controller employs a digital flight control computer to drive a set of three primary wheels and one back-up reaction wheel. Other control actuator hardware illustrated in Figure 1-1 is not used continuously on-orbit.

1.2 Special Interest

The pitch and array drive control loops are of particular interest since the moments of inertia of the body and array about the pitch axis are nearly equal. The array drive motor tends to rotate both masses equally in opposite directions. Although coupled slightly to roll and significantly to yaw through products of inertia, the low nominal body rate allows each axis to be considered separately. The complete coupling of pitch and array dynamics presents a multi-input, multi-output control problem which will be the primary consideration of this thesis.

Chapter 2 discusses several possible approaches to the control problem, the particular attractiveness of Linear-Quadratic-Gaussian (LQG) optimal theory, and outlines the proposed analysis. Chapter 3 develops

a feedback control law and considers several measurement options available to drive an estimator. Evaluation of the proposed controller against expected disturbances and the effects of neglected nonlinearities are addressed in Chapter 4. Chapter 5 presents conclusions and summarizes the structural differences between controllers designed for this loop according to a classical approach versus optimal theory.

CHAPTER 2

SURVEY OF APPROACHES AND A PROPOSAL

A variety of solutions are well suited for the control problem described in Chapter 1. Classical compensation has already been a-applied, and controllers designed with the philosophy are currently flying. It is attractive from an engineering viewpoint to consider the idea of optimal control. Solutions are based on the calculus of variations, as first noted by Wiener. An important special case, and one allowable by this problem, is linear optimal control. The techniques of linear system theory, which are well developed and powerful, may then be employed. Each approach has its strengths, and merits a more detailed discussion.

2.1 Classical Compensation

Although highly coupled, the basic attitude dynamics of the satellite are of low enough order to permit control based on classical output feedback frequency domain principles. The method's greatest strength lies in its ability to produce a fairly low order controller that is able to handle attitude dynamics which are actually quite complex with higher order effects such as flexible body modes and certain nonlinearities. Pistner, Tseng, and Muhlfelder (1975) describe how the controller currently on the satellite was developed with the aid of a multiloop frequency response simulation illustrated in Figure 2-1.

The simulation was used in the same manner as a forward transfer function. With some iteration, stabilizing compensators were developed for each loop and evaluated in terms such as phase and gain

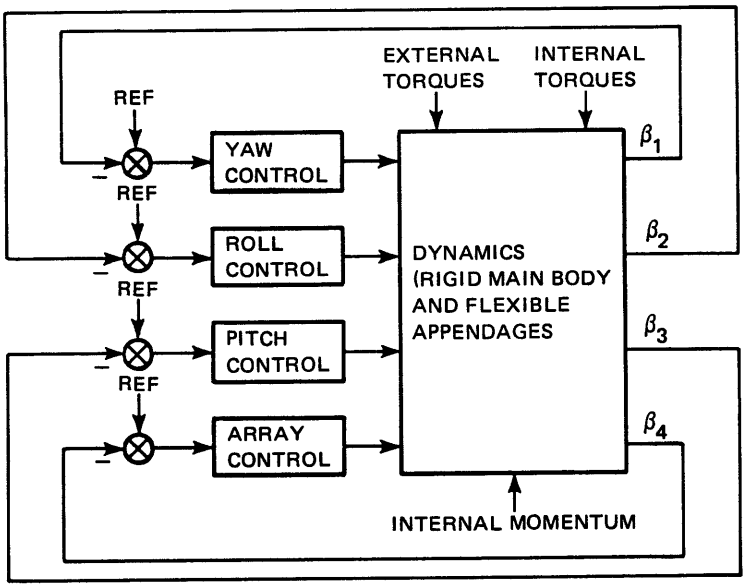

Figure 2-1. Four-loop block diagram.

margins. The effects of bending modes, inertial coupling, and computational lags could be assessed directly.

Note from Figure 2-1 that a key assumption was made at the beginning of the design procedure about the structure of the controller. Each control input is a direct function of only one output. The possibilities of cross-feeds were not considered largely because of the difficulty of having to choose gains by an iterative process. Even with this fairly low order problem, 12 additional paths would be opened.

Performance measurements such as bandwidth, phase, and gain margins are convenient and useful in the frequency domain design process. However, another, perhaps more important, class of measures exists that describes stochastic performance in terms such as mean square pointing error. These are not directly available from frequency domain synthesis techniques although they can be derived from fairly complex analytic integration of spectral densities or from Monte Carlo simulations. In the end, the final design is largely determined by the engineer's preference of easily available frequency domain parameters.

None are directly related to a measure of optimality, so the resulting design is not, in general, optimal in any sense. While it is certainly useful to be able to build a low order controller that is stable and does work, the tight constraints imposed on a satellite make it logical to seek a design that is optimal by some relevant definition, rather than settle for one that simply works.

2.2 Optimal Techniques

The key to all optimal control philosophies is the concept of a performance index. If the dynamics and control objective can be mathematically expressed in terms of a model and performance index to be extremized, powerful techniques exist to determine an optimal control. Pontryagin's minimum principle, from the calculus of variations, and the principle of optimality from Bellman's Dynamic Programming are typically applied, as discussed by Bryson and Ho (1969).

Mathematical rigor is the strength of optimal control. System constraints and dynamics are directly incorporated to determine the best control in terms of the performance index. Optimality is now an explicit goal. Of lesser but still significant importance is that optimal techniques are usually applied in the time domain. While frequency domain analysis often gives valuable insights into the problem, time domain analysis generally is more meaningful.

In reality, the rigorous optimal strategy may be difficult to determine and impossible to implement. It is not always clear how to state all control objectives, many of which are qualitative, as a mathematical function. Many of the intuitively useful performance measures, such as bandwidth, do not readily fit such an index. Not all optimal theory guarantees a solution, let alone one that fits into the framework of generally used attitude control hardware. An important special case results when system dynamics are linear, disturbances have Gaussian distributions, and the performance index is a quadratic form.

2.3 Linear-Quadratic-Gaussian Optimal Control

For a linear deterministic system and a quadradic performance index, the optimal control is easily solvable and turns out to be a linear feedback of all state variables. However it is usually the case that not all state variables can be directly measured, and those that can be are corrupted by noise. If the measurement noises and the disturbances acting on the system are adequately modeled by uncorrelated Gaussian random processes, then subject to certain constraints, Kalman (1960) showed that the optimal state estimate in terms of mean square error is derived with a linear filter. Furthermore, Joseph and Tou (1961) proved that the minimum mean square error controller is Kalman's estimator cascaded with the feedback control law based on deterministic full state knowledge. This unusual and interesting result permits the design process to be broken into two theoretically independent stages. Multiple inputs and multiple outputs are assumed in general, which is an important distinction between this method and classical techniques.

Note that none of the arguments for mathematical rigor have been lost. The LQG case just admits a most tractible solution. Quadratic performance measures can be physically meaningful when representing quantities such as mean-square pointing error and control power. That stochastic performance is directly evaluated is another attraction. Although implementation of the optimal LQG controller typically requires more computation than a classical output feedback controller, the dimension of the linear optimal controller is bounded to no more than the dimension of the system modeled. In the case of a time invariant system, and for times sufficiently far from initial and terminal, the optimal filter and controller gains are fixed allowing simpler inplementation. Finally, linear system theory is well developed so evaluation of a proposed controller's response, stability, and stochastic performance is easily done.

Even bounded dimensionality (which is not necessarily the case for all optimal control techniques) is not the same as easy implementation. Unlike classical techniques, which can handle high order dynamics

with a low order controller, a rigorously optimal linear controller generally requires each state to be estimated and fed back. In a study of optimal control of the three rigid body modes, not including direct control of array rotation, and several significant flexural modes of this satellite by Tseng and Tracy (1977), 19 states were required. This is a good bit higher than desirable for the present flight control computer. Nonlinear effects are not as directly incorporated as was done in the classical design. Although it is justified to linearize rotational dynamics about the on-orbit nominal attitude, many significant nonlinearities are hard discontinuities and must be neglected. The assumption of uncorrelated Gaussian disturbances is difficult to fit to the true disturbance environment. Despite these drawbacks, linear optimal theory presents the most attractive approach to applying an optimal technique.

2.4 Proposal

The pitch and array loops are directly coupled, hence they offer the most interesting possibilities for exploiting optimal control techniques. It is possible to consider pitch axis dynamics separately so the control problem becomes linear. The implications of this assumption will be evaluated later. Gaussian assumptions can be made and justified for the disturbances acting on the satellite and controller. The objective of this thesis is to synthesize a realizable optimal control law for the pitch and array loop, and address the important implementation issues such as estimation, closed loop performance, and controller complexity. Neglected nonlinear effects must also be considered. Since the proposed approach is an optimal technique, improved performance is expected where direct comparisons can be made to the existing control design.

Although much of this thesis is involved with the LQG design process, contrasting the results of this approach to those derived by classical techniques is also an important objective. Such comparisons are a means to further the practical understanding of modern control. Both techniques result in linear feedback filters that operated on the same

satellite. It is possible to model the current controller as a gain matrix allowing it to be analyzed with the vector-matrix algebra normally employed by modern theory. The optimal controller, on the other hand, can be illustrated in the block diagrams of classical theory which clearly illustrate structural differences. Such comparisons can be more meaningful than purely quantitative performance measures for accomplishing this less direct goal of the thesis.

CHAPTER 3

THEORETICAL LINEAR SYNTHESIS AND ANALYSIS

An important practical result of the theorem derived by Joseph and Tou (1961) is that the optimal deterministic controller and state estimator can be designed separately. A model is derived and an optimal control law and optimal estimator are specified in this chapter. Several measurement schemes, using gyros or star mappers or a combination of both are evaluated. Practical concerns as illustrated by eigenvalue locations, dictate that although filter and control law designs are done separately, they should not be done independently. Finally, the complete closed-loop linear system is evaluated under linear assumptions.

3.1 Deterministic Control

Under the assumption of perfect state knowledge, the optimal control in terms of minimizing a quadradic performance index in state and control turns out to be a linear feedback of current state. In general, the optimal gains are time varying. If plant parameters are fixed, and the terminal time is indefinitely in the future, which is the case for this on-orbit controller, the feedback gains become constant. The primary synthesis task, for a given model, is accurately stating control objectives as a performance index and calculating feedback gains.

3.1.1 Model

A linear model is assumed of the form

$$\underline{x}_{i+1} = \Phi \underline{x}_i + \Lambda \underline{u}_i \tag{3-1}$$

where Φ is the state transition matrix and Λ is the control effectiveness matrix. The state, $\underline{x}$, and control, $\underline{u}$, vectors are defined as follows:

$$\underline{x} = \begin{bmatrix} q \\ \phi \\ \omega \\ \theta \\ \dot{\theta} \\ h \end{bmatrix} \quad \begin{array}{l} \text{Integral of attitude error (rad-s)} \\ \text{Pitch error (rad)} \\ \text{Pitch rate (rad/s)} \\ \text{Solar array angle error (rad)} \\ \text{Solar array rate (rad/s)} \\ \text{Reaction wheel momentum (in.-lb-s)} \end{array}$$

$$\underline{u} = \begin{bmatrix} u_1 \\ u_2 \end{bmatrix} \quad \begin{array}{l} \text{Command voltage to reaction wheel (volts)} \\ \text{Command torque to SAD motor (in.-lb)} \end{array}$$

Detailed model development specifying Φ and Λ is contained in Appendix A. Key assumptions are that the satellite and array are rigid bodies, the reaction wheel dynamics are first order, and the array motor is a perfect torque transducer.

3.1.2 Performance Index

A scalar cost function is defined in the form

$$c = \sum_{i=1}^{L-1} \left\{ \underline{x}_i^T Q_{xx} \underline{x}_i + \underline{u}_i^T R_{uu} \underline{u}_i \right\} + \underline{x}_L^T Q_L \underline{x}_L \tag{3-2}$$

Widnall (1968) suggests that this cost should include a term of the form $\underline{x}_i^T S \underline{u}_i$. Such a term becomes important in suppressing hidden oscillations that may arise if closed-loop poles have frequencies near

the Nyquist limit. Since the closed-loop dynamics desired for attitude control are much less than 1 Hz, which is half the computer sample rate, the cross weighting will be ignored and the cost left in the form of Eq. (3-2).

Choosing the symmetric weighting matrices in Eq. (3-2) determines the closed-loop performance for a particular plant. Since the terminal time is not relevant, Q_L, the weight placed on the terminal state, may be arbitrary, but 24 free parameters are still left in Q_{xx} and R_{uu}. A common approach in optimal control design is trial and error, proposing weighting matrices and evaluating time responses and pole locations until an adequate design is reached. While there is no reason such an approach cannot converge to a good design, the number of permutations for even this low-order system is enormous. It also seems that this defeats some of the advantages of optimal control by forcing the response to conform to some predetermined idea of what a good response should be and fitting a performance index to that rather than in reverse order.

The control objective of Section 1.2 can be restated in the following manner: satellite attitude stabilization requires that body rotation energy be controlled, angular errors nulled, and that finite control power is expended in the process.

The rotational energy of the body is $1/2I_b\omega^2$, and the energy of the array is $1/2I_a(\omega + \dot{\theta})^2$, so the performance index should contain the following terms penalizing kinetic energy,

$$1/2(I_b + I_a)\omega^2 + I_a\omega\dot{\theta} + 1/2I_a\dot{\theta}^2$$

Penalties on angular errors will insure the controller works to null these errors. Widnall (1968) notes that penalty terms of the form $1/2I_b\omega_b\phi^2$ and $1/2I_a\omega_a\theta^2$ will result in closed-loop mode frequencies near ω_b and ω_a, respectively. To make integral feedback effective, the cost

must also include a term of the form Wq^2. There is little a-priori motivation for choosing W, so it will be determined experimentally. Reaction wheel speed should not be penalized since it should absorb all undesirable momentum and, in general, spins continuously.

As it turns out from the scaling of the system, SAD commands have about 10 times the control authority as a numerically equal reaction wheel command. It is desirable to keep wheel speed changes a minimum, so the diagonal elements of R_{uu} will be set equal, and their values experimented with until the loop response speed is fast enough but does not saturate actuator limits.

3.1.3 Solution of Optimal Control

Kalman and Koepcke (1958) originally proposed a solution to a class of control problems represented by Eq. (3-1) and (3-2), but with scalar control u, by dynamic programming. Extending their work to the case of a vector control, Widnall derived a recursion that minimizes Eq. (3-2). The optimal control turns out to be a linear feedback of the state vector in the form

$$\underline{u}_i = -F_i \underline{x}_i \tag{3-3}$$

where the feedback gain matrix F_i is found by the backwards recursions

$$F_i = \left[\Lambda^T P_{i+1} \Lambda + R_{uu}\right]^{-1} \Lambda^T P_{i+1} \Phi \tag{3-4}$$

$$P_i = \left[\Phi - \Lambda F_i\right]^T P_{i+1} \left[\Phi - \Lambda F_i\right] + Q_{xx} + F_i^T R_{uu} F_i$$

$$i = L, L-1, \ldots, 1, 0 \tag{3-5}$$

with P_L initialized to Q_L. A derivation of Eq. (3-4) and (3-5) is in Appendix B.

3.1.4 Results

With some experimentation, a choice of weighting matrices as follows:

$$Q_{xx} = \begin{bmatrix} 5 & 0 & 0 & 0 & 0 & 0 \\ 0 & 44.6 & 0 & 0 & 0 & 0 \\ 0 & 0 & 884 & 0 & 439 & 0 \\ 0 & 0 & 0 & 22 & 0 & 0 \\ 0 & 0 & 439 & 0 & 440 & 0 \\ 0 & 0 & 0 & 0 & 0 & 0 \end{bmatrix}$$

$$R_{uu} = \begin{bmatrix} 0.1 & 0 \\ 0 & 0.1 \end{bmatrix}$$

resulted in an attractive closed-loop system. Values of Q_{xx} correspond to a choice of $\omega_a = 0.05$ rad/s and $\omega_b = 0.1$ rad/s as discussed in Section 3.1.3. Elements of R_{uu} were adjusted until overall response speed was on the order of the current control law.

As was noticed by Tseng and Tracy (1977) in a study of optimal control of the flexible modes of this spacecraft, the response showed greatest sensitivity to the integral penalty. Increasing integral cost resulted in a faster but more oscillatory response.

The closed-loop eigenvalues for the specific weightings selected are plotted in Figure 3-1. Note that one closed-loop pole appears directly at $z = 1$. This is a result of the fact that the system is not fully controllable. All angular momentum along the pitch axis must appear as body rate, array rate, or in the reaction wheel. Since external torques are not available to the controller, the total angular

momentum cannot change, but eventually ends up in the reaction wheel. A closed-loop pole at z = 1 is the mathematical indication that one state will in steady state be non-zero, depending on initial conditions.

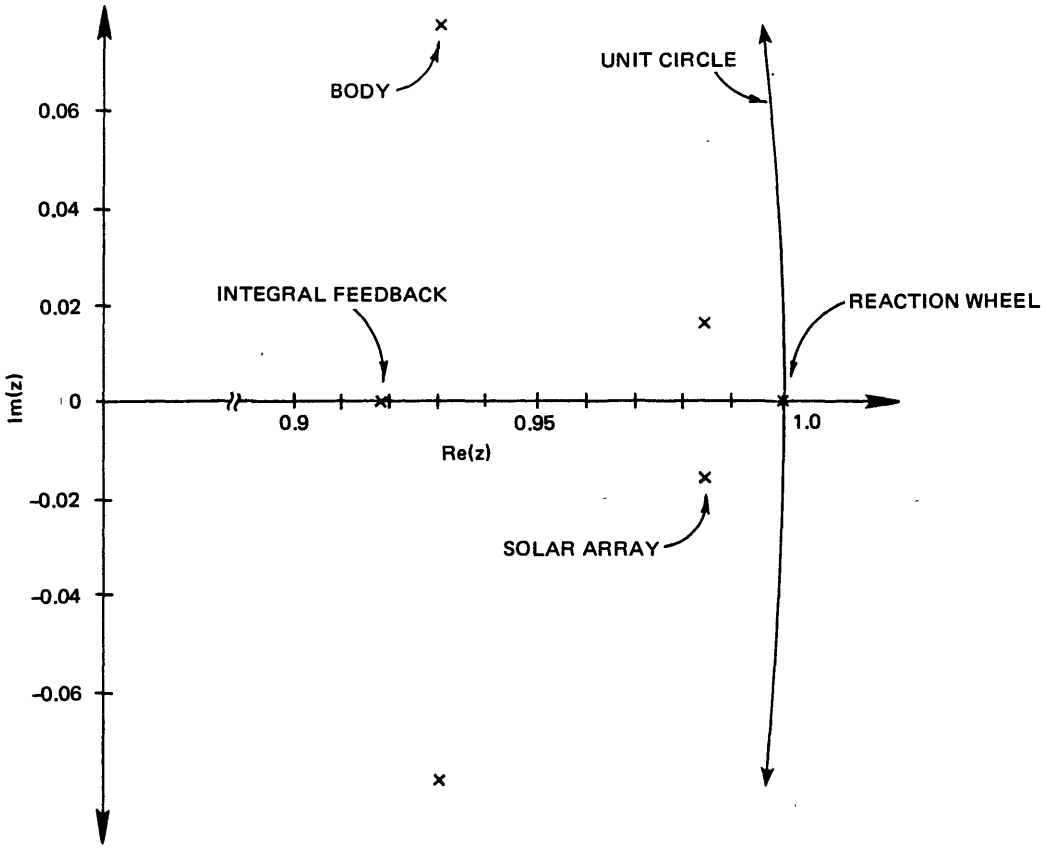

Figure 3-1. Closed-loop eigenvalues.

The body modes have a closed-loop natural frequency of 0.217 rad/s, and the array frequency is 0.0457 rad/s, which are quite close to the frequencies used to formulate array and body deviation penalty terms.

The optimal gain matrix is

$$F = \begin{bmatrix} 1.247 & 40.30 & 962.8 & 14.31 & 456.6 & 0.01378 \\ -6.204 & -69.58 & -296.7 & 2.701 & 36.12 & 0.0001018 \end{bmatrix}$$

Although an exact comparison of gains is not possible because the current SAD compensator has dynamics, if state feedback is chosen that approximates dominant array behavior, then the current control law is represented by the following gain matrix. Body gains are exact.

$$F = \begin{bmatrix} 17.57 & 350.46 & 2336.4 & 0 & 0 & 0 \\ 0 & 0 & 0 & 265.0 & 418.9 & 0 \end{bmatrix}$$

Figure 3-2 is the response of the satellite under optimal control to an initial pitch error of 1°. Notice how the control law uses the solar array drive to twist the satellite in a manner like a cat in free-fall throwing its hindquarters one way to turn its head and forlimbs the other.

Contrast this response with Figure 3-3 which is the response to the same conditions but operating under the current control law. Note that even though the response speed is slower, since the reaction wheel alone must reorient the entire spacecraft, peak wheel momentum is approximately five times higher. Under the current control law the array drive is used only to maintain array orientation, and is not able to assist in controlling the satellite body.

The primary job of the on-orbit control system is to maintain attitude in the face of disturbance torques. Worst-case external torques are estimated by the manufacturer to be as follows, acting on the array

$$Td_a = \underbrace{\left[0.0906 + 1.21 \sin 2\beta \right]}_{\text{(gravity gradient)}} \times 10^{-3} \text{ in.-lb}$$

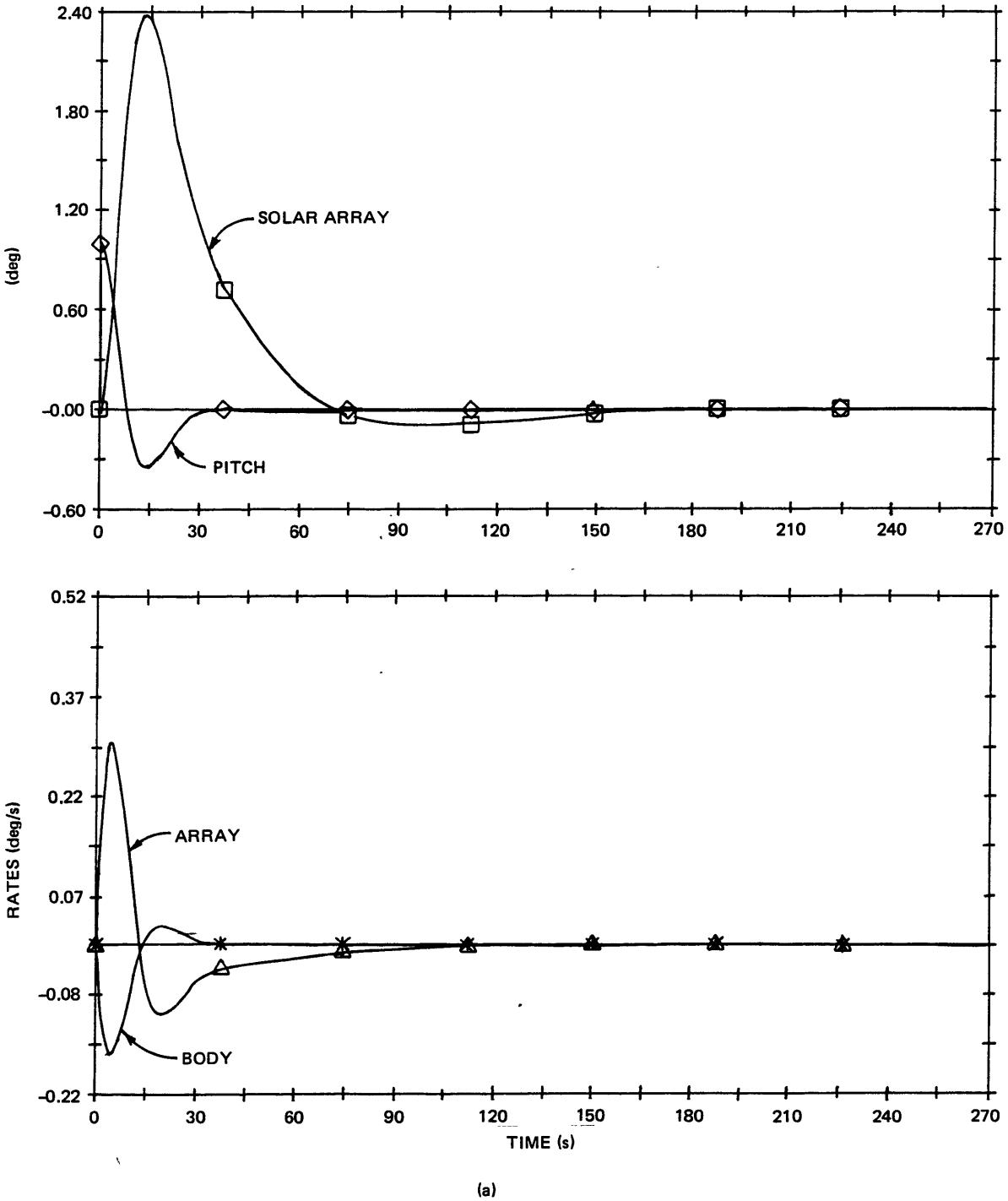

Figure 3-2. Deterministic optimal control, response to initial conditions.

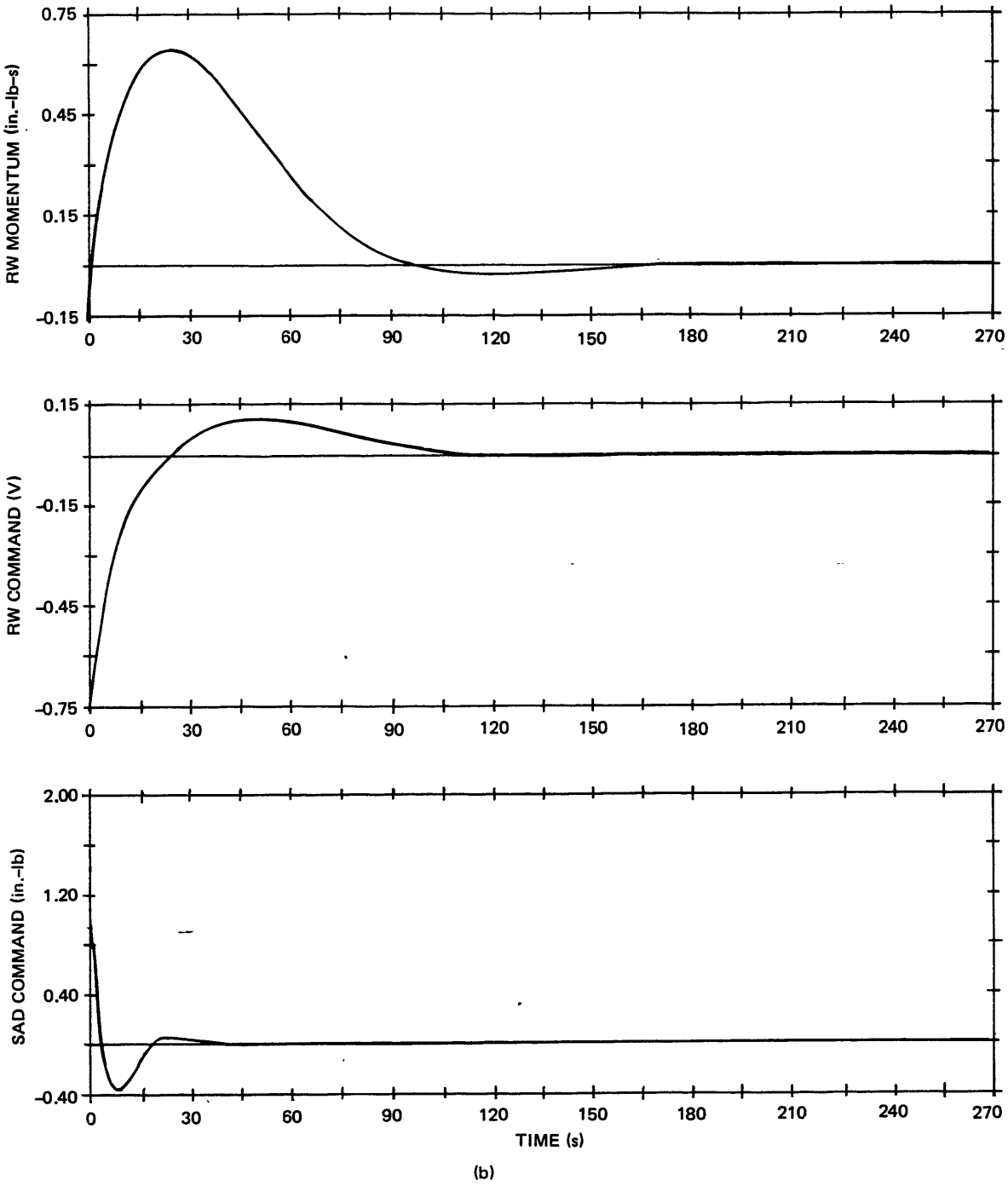

Figure 3-2. Deterministic optimal control, response to initial conditions. (Cont.)

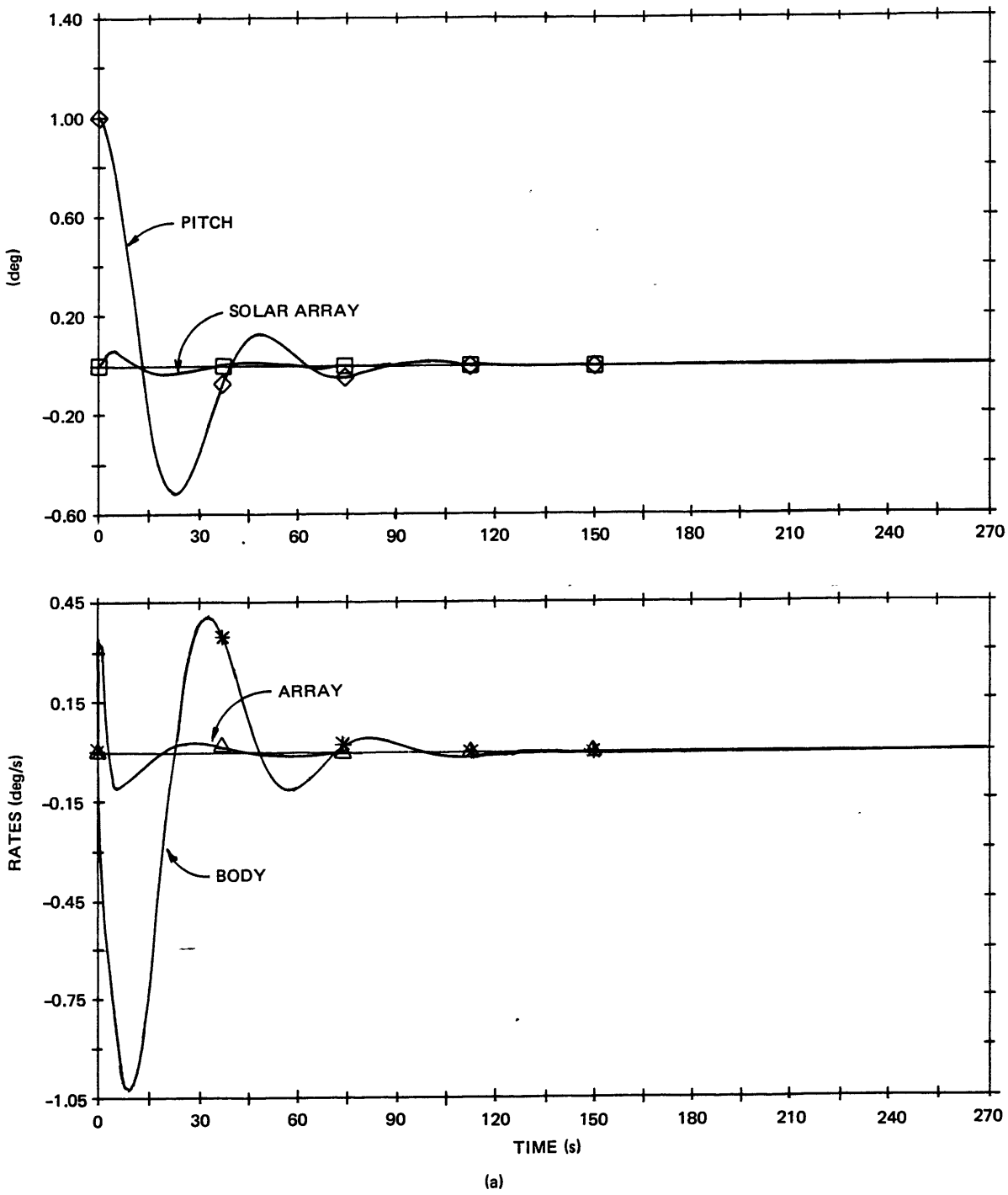

Figure 3-3. Current control law, response to initial conditions.

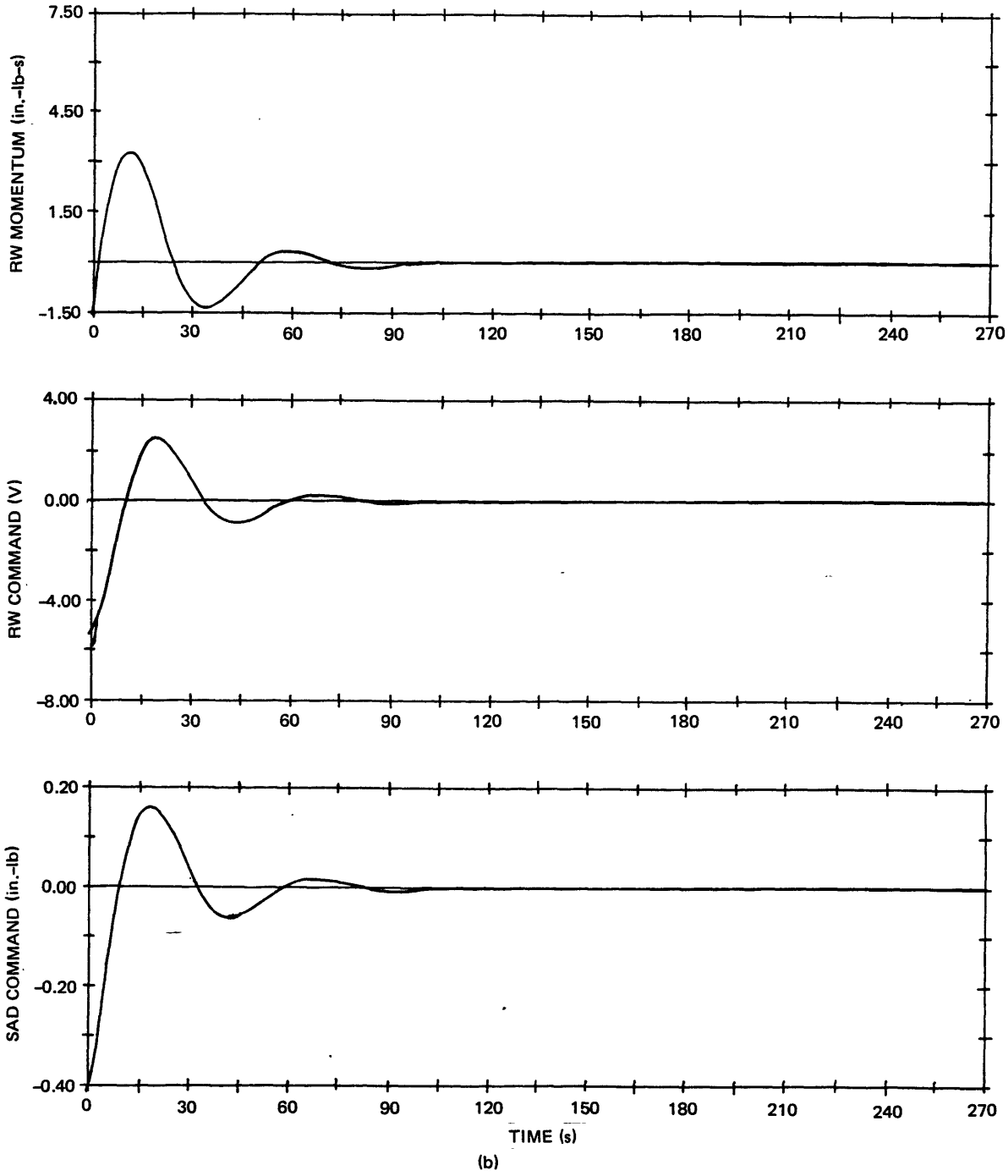

Figure 3-3. Current control law, response to initial conditions. (Cont.)

acting on the body

$$Td_b = \Big[\underbrace{-0.22 \sin \beta}_{\text{solar pressure}} + \underbrace{0.212 \sin (\beta - 26.6°)}_{\text{magnetic residual}}\Big] \times 10^{-3} \text{ in.-lb}$$

where β is the orbit anomaly, and for circular orbits is nominally given by

$$\beta(t) \approx \omega_0 t \qquad \omega_0 = 0.06°/s$$

Figure 3-4 is the loop response under optimal control to worst-case external disturbances over a full orbit, and Figure 3-5 illustrates the response under the existing control law. Important differences in the responses are that under optimal control pitch error peaks at 0.07 arc-sec while the current controller allows peak errors of 0.4 arc-sec. Such a result is not free. The optimally controlled solar array deviates up to 180 arc-sec, while the current control system keeps array errors under 1 arc-sec, however this produces no real benefit, since the solar array only has to point to within 3 degrees of the sun line.

Optimal control is able to produce a superior response in the pitch loop. The non-zero gains of the current law are all significantly higher than the corresponding optimal gains, however, the lower, but optimally distributed, gains actually produce tighter control and faster response of body orientation than the current law. Control authority is shifted away from the reaction wheel onto the array drive. Exploiting the multi-input nature of the loop is the most powerful feature of optimal control, and is done automatically in a way that would not be the result of a classical approach to the problem.

While the classical approach operates only on directly measurable quantities, full state knowledge is required to implement an optimal controller. Either all state variables must be instrumented, or an estimator developed to operate with available measurements.

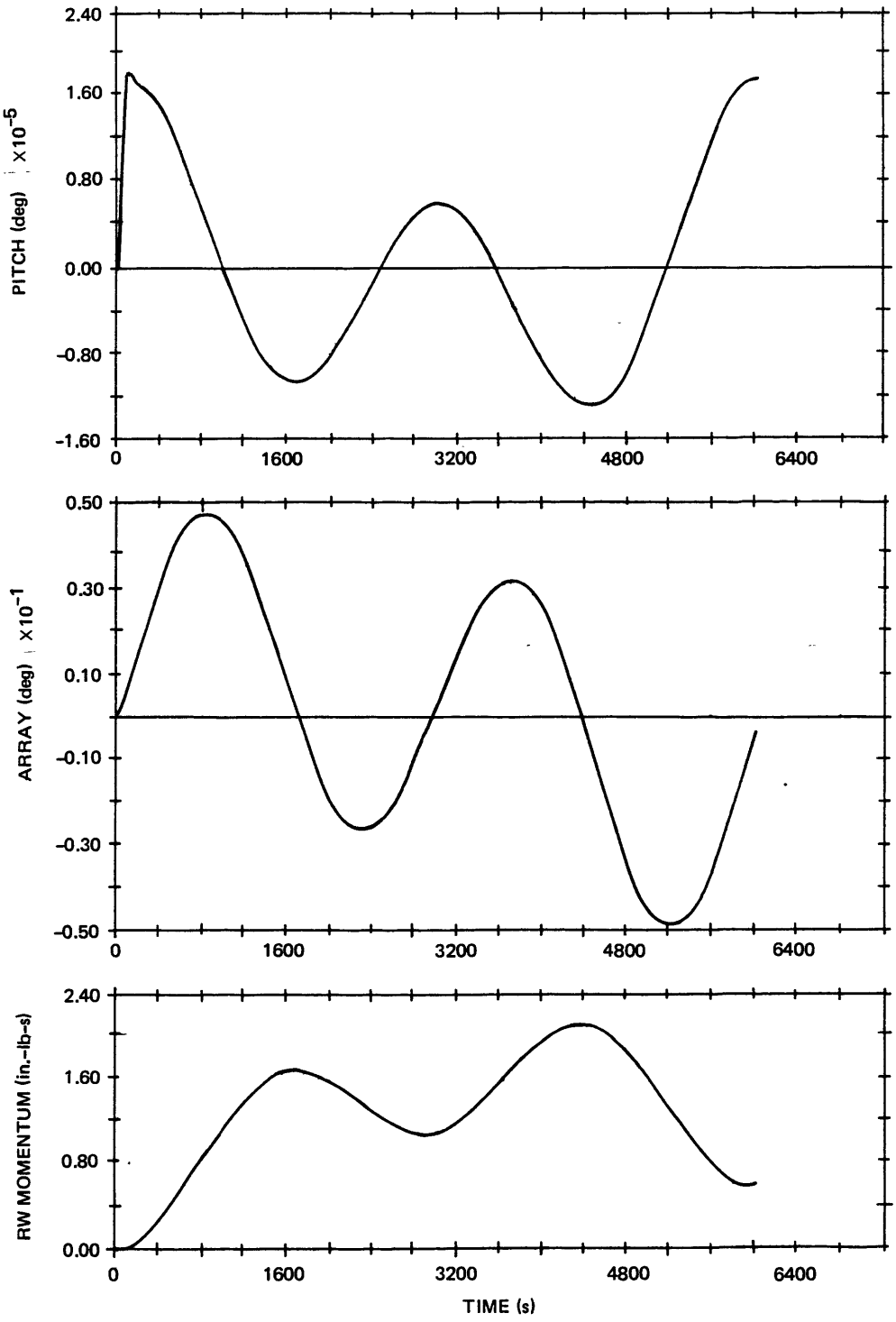

Figure 3-4. Deterministic optimal control, worst-case external torques.

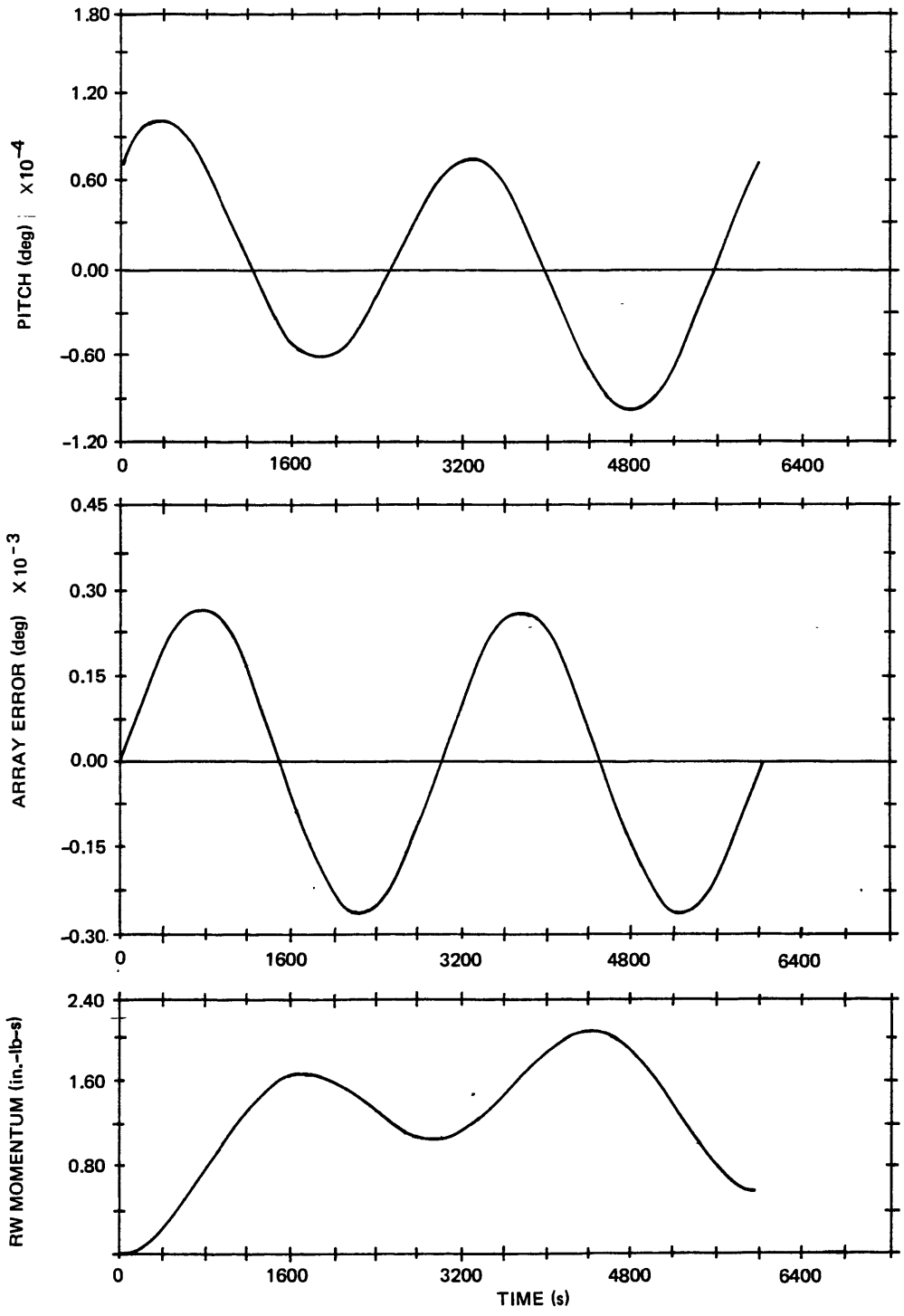

Figure 3-5. Current control law.

3.2 Stochastic Estimation

3.2.1 Approach

Most of the state variables defined in the previous section are directly instrumented by sensors on the satellite. Changes in inertial orientation are measured by a set of rate integrating gyros, updated by a star sensor to bound gyro drift, which also produce attitude rate information. The solar array orientation is reported directly, although its rate is not. Reaction wheel speed (a measurement differing from actual momentum only by a scale factor of wheel inertia) is monitored, so excess momentum can be dumped via magnetic torquing coils. With this nearly complete set of measurements, an obvious approach is to calculate the two remaining states, by back-differencing array angles and numerically integrating attitude error, then using the measurements directly with appropriate feedback gains. Why bother with more sophisticated estimation techniques if the requirement for full state feedback can be met so directly?

The answer to this question is that the measurements are corrupted to widely varying degrees by noise, and direct feedback would amplify the effect of sensor errors. Most of the noise would originate from the wheel and array sensors, with angular errors several orders of magnitude higher than gyros or star mappers. However, the value of high-quality inertial measurements is lost if they are mixed directly with much noisier signals. In addition, it is often the case that a state can be estimated better than it can be directly measured.

Athens (1971) discusses another justification for an estimator based on the implications of assuming a linear model for a process that is not linear. The error statistics used in estimation theory enable an engineer to account for nonlinear and higher-order linear effects by modeling them as random, and to be able to quantify the level of uncertainty in the model. As a result, the state estimate presented to the control law follows a trajectory that is appropriate for the feedback gains, having unmodeled modes attenuated.

Linear optimal filtering theory is applied to estimate the state vector from available measurements. For a linear stochastic system modeled by

$$\underline{x}_{i+1} = \Phi \underline{x}_i + \Lambda \underline{u}_i + \Gamma \underline{w}_i \tag{3-6}$$

which is Eq. (3-6) but including a random forcing function, w_i, characterized by

$$E\left[\underline{w}_i\right] = 0 \qquad E\left[\underline{w}_i \underline{w}_j^T\right] = Q\delta_{ij}$$

where Γ, the disturbance weighting matrix, is calculated in Appendix A, and measurements corrupted by noise

$$\underline{y}_i = H\underline{x}_i + \underline{v}_i \tag{3-7}$$

$$E\left[\underline{v}_i\right] = 0$$

$$E\left[\underline{v}_i \underline{v}_j^T\right] = R\delta_{ij}$$

$$E\left[\underline{w}_i \underline{v}_j^T\right] = 0$$

The optimal estimate $\hat{\underline{x}}$, in the sense of mimimum mean-square estimation error, and the covariance of the estimation error, P, is propagated between sample times by

$$\hat{\underline{x}}_i^- = \Phi \hat{\underline{x}}_{i-1}^+ + \Lambda \underline{u}_{i-1} \tag{3-8}$$

$$P_i^- = \Phi P_{i-1}^+ \Phi^T + \Gamma Q \Gamma^T \tag{3-9}$$

At sample times, the estimate and error are updated by

$$\begin{aligned} \hat{\underline{x}}_i^+ &= \hat{\underline{x}}_i^- + K_i[\underline{y}_i - H\hat{\underline{x}}_i^-] \\ P_i^+ &= (I - K_iH)P_i^-(I - K_iH)^T + K_iRK_i^T \end{aligned} \tag{3-10}$$

where the Kalman gain matrix, K_i, is calculated each interval by

$$K_i = P_i^-H^T\left[HP_i^-H^T + R\right]^{-1} \tag{3-11}$$

Derivation of Kalman's equations in this form is not presented, but are as found in Gelb (1974) or Jazwinski (1970).

3.2.2 Stochastic Modeling

Given a particular model, the behavior of the filter is shaped entirely by the disturbance matrices Q and R. In this case, external disturbances enter the system as random torques acting on the satellite body, solar array, and reaction wheel. Measurements fall into two classes, internal and external, the former including the wheel and solar array, while the latter determine inertial orientation. This distinction is made because external pointing accuracy is the control objective, requiring the best knowledge of sensor error, while the internal modes are not particularly important. Fortunately, measurement error is well known on all of the proposed external sensors, so meaningful results are possible. Little is known about array and wheel sensor accuracy because they were not intended to be used in an attitude estimator. A conservative approach will be used in modeling these sensors, that is, the ratios of disturbance to sensor noise will be chosen to run the filter as slow as possible without interfering with the controller eigenvalues. A slow filter has low gains, which implies at each sample time less of any random error is able to enter the system. As long as the

filter eigenvalues are faster than the desired closed-loop eigenvalues, the response should be satisfactory, and in fact, the filter really doesn't need to run any faster.

External sensors of interest are the existing rate integrating gyroscopes, a 2-D star mapper (such as a charge-coupled device (CCD)), and pure rate sensing gyros.

Truncale, Koenigsberg, and Harris (1972) conducted tests on several gyros including a Nortronics K7G-3C which is the same type of instrument as the K7G-3K used on the spacecraft. The linearized power spectral density of gyro noise is plotted in Figure 3-6.

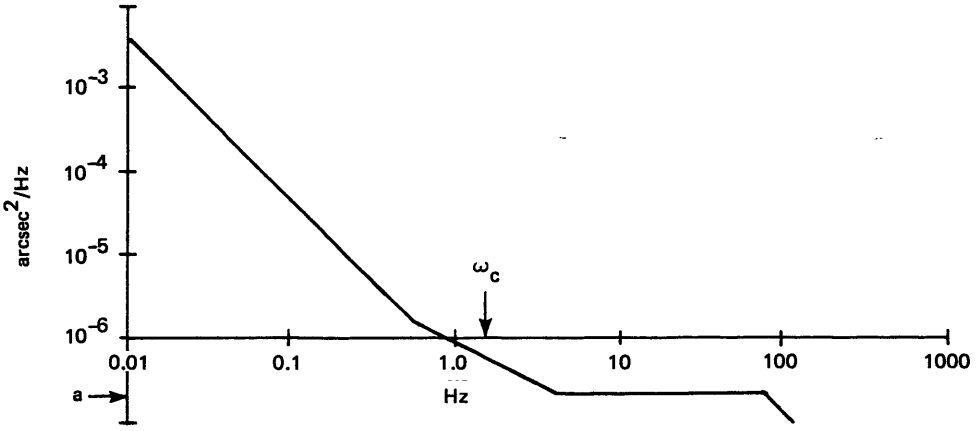

Figure 3-6. Gyro noise power spectral density.

The major difference in the K7G-3C tested and the K7G-3K is the former's wheel momentum is 180,000 gm-cm^2/s while the latter's is 60,000 gm-cm^2/s, and consequently has a lower scale factor and higher sensitivity to torque disturbances. Since the test environment was reported to be a major source of the noise, it is certain that Figure 3-6 is pessimistic and will be taken to represent the 3K gyro as well.

A linear system driven by white noise of indicated spectral densities is used to model gyro noise, and is diagrammed in Figure 3-7.

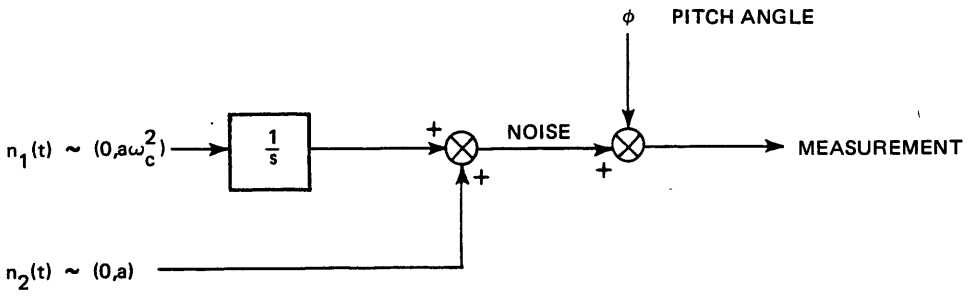

Figure 3-7. Gyro noise model.

Parameter "a" is the high frequency spectral intensity of the gyro noise and ω_c is the break frequency of the low frequency portion of the spectrum.

However, a continuous time model does not fit into the filter structure, so the sample data representation of the system in Figure 3-7 must be determined. Let x(t) be the output of the integrator, modeling gyro drift. At discrete sample intervals, the following difference equations model the continuous process

$$x_{i+1} = x_i + n_{1i} \tag{3-12}$$

$$y_i = \phi_i + n_{2i} \tag{3-13}$$

y_i is the sampled measurement, and n_{1i} and n_{2i} are white random sequences. n_{1i} is given by the integral

$$n_{1i} = \int_0^{\Delta T} n_1(\tau)\, d\tau \qquad E[n_1(t)n_1(t+\tau)] = N_1\delta(\tau)$$

$$N_1 = \pi a\omega_c^2$$

which is equivalent to the simple Ito integral

$$n_{1i} = \int_0^{\Delta T} d\beta \qquad E[d\beta^2] = N_1\, dt$$

The mean of any Ito integral is zero, so $\overline{n_{1i}} = 0$, and the auto-correlation is calculated by

$$E[n_{1i}n_{1j}] = \int_{t_i}^{t_{i+1}} d\beta \int_{t_j}^{t_{j+1}} d\beta$$

$$= \begin{cases} \displaystyle\int_{t_i}^{t_{i+1}} N_1\, dt & i = j \\ 0 & i \neq j \end{cases}$$

$$E[n_{1i}n_{1j}] = q_g\, \delta_{ij} = \pi a \omega_c^2\, T\, \delta_{ij} \qquad (3\text{-}14)$$

using the cross correlation properties of two Ito integrals.

n_{2i} is not as clear since it is an attempt to model a directly measured white continuous process with a white random sequence. One approach might be to determine the spectral density of a random sequence and match it to the high frequency spectral density of the gyro. Unfortunately, a random sequence like n_{2i} with fixed change times is not stationary but has an auto correlation function as shown in Figure 3-8. A power spectral density is defined only for stationary random processes. If, however, the random sequence had a random phase, by allowing the start time to be uniformly distributed over $(0,\Delta T)$, the auto correlation of the process would be a function only of time difference between t_1

and t_2, and the process would be stationary. Defining $\tau = t_1 - t_2$, the autocorrelation function may be plotted as in Figure 3-9.

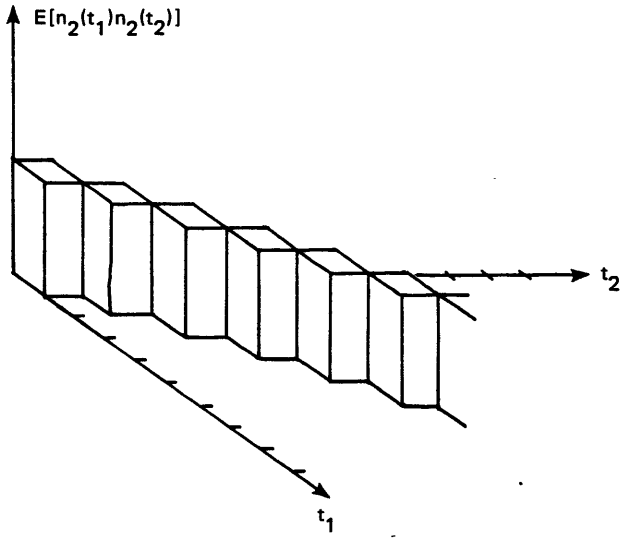

Figure 3-8. Fixed phase random sequence correllation.

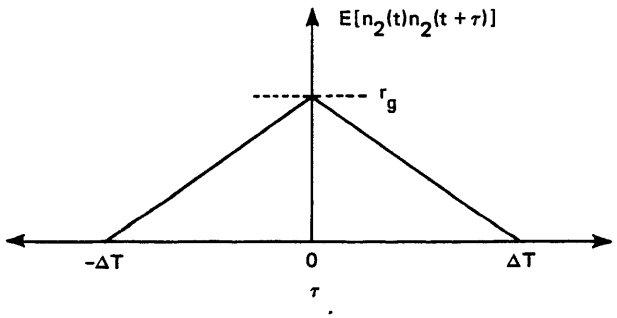

Figure 3-9. Random phase random sequence correllation.

A power spectral density may now be calculated, and adopting Laning and Battin's (1956) convention is given by,

$$\Phi_{22}(\omega) = \frac{1}{\pi}\int_{-\infty}^{\infty} E[n_2(t)n_2(t+\tau)]e^{-j\omega\tau}\,d\tau$$

$$= \frac{2r_g}{\Delta T \pi \omega^2}[1 - \cos \omega\Delta T] \qquad (3\text{-}15)$$

Figure 3-10 plots $\Phi_{22}(\omega)$.

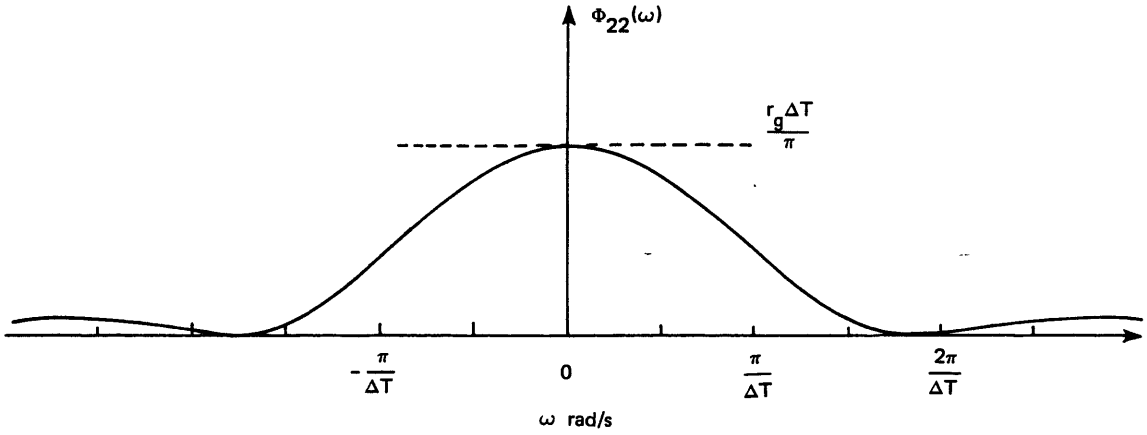

Figure 3-10. Random phase random sequence power spectral density.

Although this spectral density is not exactly applicable to the random sequence used in modeling, it seems reasonable that since the fixed start time sequence is a special case of the uniform start time sequence, the two would have similar effects over the long run on the system they were driving. To finish specifying the stochastic gyro model, r_g is chosen so that the low frequency limit of the random sequence spectral density matches the flat portion of the gyro noise spectral density.

$$r_g = \frac{\pi a}{\Delta T} \tag{3-16}$$

Note the different way π and ΔT appear in Eq. (3-14) and (3-16). Sequence n_{1i} directly simulates a white noise, while n_{2i} models the increasing uncertainty of an integrator driven by white noise. The latter is upon much firmer mathematical ground.

A second external sensor of interest is a 2-D star mapper. The proposed device is a 324 × 324 pixel CCD with an 8° × 8° field of view. In its primary mode, the star mapper tracks a cataloged star, and by comparing known location with the image location, the star mapper directly calculates inertial attitude. Alternately, the star mapper could track unknown stars and derive body rates, an idea that is studied by Gai, et al. (1980) but will not be considered here.

Each pixel has an 88.8 arc-sec field of view. If a star's image is defocused over a 3 × 3 block of pixels, the centroid of the image can be calculated to considerably better than one pixel's resolution. Gray and Youmans (1979) derived estimates of the measurement error of a CCD type star mapper using optical components similar to that currently installed on the spacecraft. For the case of one known star and one image sample, their results are summarized in Table 3-1.

Table 3-1. Image centroid error.

Star Magnitude	Standard Deviation
0	0.13 (arc-sec)
+1	0.32
+2	0.79
+3	2.00
+4	4.99
+5	12.56
+6	31.40

Since 5^{th} magnitude stars are near the lower limit of sensitivity, the 12.56 arc-sec error for such stars will be considered to be the worst-case error when considering star mapper measurements in the estimator.

Both the gyro and star mapper are able to supply data faster than the 2-Hz rate the estimator in the flight computer requires. It may be useful to directly calculate body rates by differencing an attitude measurement taken in a short time, say 0.1 second, before a major computer cycle with the attitude measurement taken at the sample and command time. The error in such a derived measurement is now calculated.

Define an attitude measurement at t_i, a major computer cycle, and at t_i' taken Δt earlier, where ϕ is the pitch angle

$$\hat{\phi}_i' = \phi_i' + n_i' \qquad E[n] = 0$$

$$\hat{\phi}_i = \phi_i + n_i \qquad E[n_i n_j] = r\delta_{ij}$$

$$\Delta t = t_i - t_i'$$

Then a direct estimate of body rate is

$$\hat{\omega}_i = \frac{1}{\Delta t}\left[\hat{\phi}_i - \hat{\phi}_i'\right] \tag{3-17}$$

Assume that a random constant zero mean acceleration, a, of variance σ_a^2 acts over Δt. Given the true rate ω and attitude ϕ at t_i', then the true rate and attitude at t_i is

$$\omega_i = \omega_i' + \alpha\Delta t \tag{3-18}$$

$$\phi_i = \phi_i' + \omega_i'\Delta t + 1/2a\Delta t^2 \tag{3-19}$$

The mean of $\hat{\omega}$ is

$$
\begin{aligned}
E[\hat{\omega}] &= \frac{1}{\Delta t} E\left[\phi_i - \phi_i' + n_i - n_i'\right] \\
&= \frac{1}{\Delta t} E\left[\phi_i' + \omega_i'\Delta t + 1/2a\Delta t^2 - \phi_i' + n_i - n_i'\right] \\
&= E[\omega_i - a\Delta t] \\
&= \omega_i
\end{aligned}
\tag{3-20}
$$

so the estimate is unbiased. Assuming a, n_i, and n_i', are uncorrellated, the covariance of $\hat{\omega}$ is

$$
\begin{aligned}
E[(\hat{\omega} - \bar{\hat{\omega}})^2] &= E\left\{\left[\frac{1}{\Delta t}(\omega_i'\Delta t + 1/2a\Delta t^2 + n_i - n_i') - \omega_i'\right]^2\right\} \\
&= \frac{1}{4}\sigma_a^2 \Delta t^2 + \frac{2r}{\Delta t^2}
\end{aligned}
\tag{3-21}
$$

The random acceleration, a, is actually a process noise, so the back-difference rate measurement error introduces a correlation between measurement and process noise when it is used. Typical worst-case torque disturbances are on the order of 1 in.-lb, standard deviation. For star-mapper measurement errors of 12.56 arc-sec and a hold time of 0.1 second, the rms error introduced by the random torque is 11.6 arc-sec/s, while the sensor noise itself introduces an error of 178 arc-sec/s into the rate estimate, so the correlation is not too significant. Such is not the case if gyro measurements are used. Two gyro samples taken 0.1 second apart could estimate rate to 0.04 arc-sec/s if no disturbing torques were present. One approach to determining the effect of process/measurement correlation is to rederive the filter equations retaining this assumption. Jazwinski (1970) presents two such cases, but assumes a different timing convention than that of Eq. (3-6). A simpler solution, and one that allows

use of filter Eq. (3-8) through (3-11), is to augment that state vector and redefine the measurement. Without taking the expectation in Eq. (3-20), the direct rate estimate may be written as

$$\hat{\omega} = \frac{1}{\Delta t}\left[\omega_i'\Delta t + 1/2a\Delta t^2 + n_i - n_i'\right]$$

$$= \omega_i - a\Delta t + 1/2a\Delta t + \frac{n_i - n_i'}{\Delta t}$$

$$\hat{\omega} = \omega_i - 1/2a\Delta t + \frac{n_i - n_i'}{\Delta t} \tag{3-22}$$

The acceleration that acts from t_i' to t_i is

$$a(t_i', t_i) = \frac{T_{db_{i-1}}}{I_b} \tag{3-23}$$

Since the random torque introduced at t_{i-1} is modeled as constant over the interval (t_{i-1}, t_i). Define a state variable

$$x_{i+1} = T_{db_i} \tag{3-24}$$

Elements of Eq. (3-22) are now all state variables and measurement noises that are uncorrelated with the process noise. The variance of the noise in Eq. (3-22) is

$$E\left[\left(\frac{n_i - n_i'}{\Delta t}\right)^2\right] = \frac{2r}{\Delta t} \tag{3-25}$$

Note also that the noise in Eq. (3-22) is correlated with the attitude measurement noise at time t_i

$$E\left\{\left[\hat{\phi}_i - E(\hat{\phi}_i)\right]\left[\hat{\omega}_i - E(\hat{\omega}_i)\right]\right\} = E\left[n_i\left(\frac{n_i - n_i'}{\Delta t}\right)\right]$$

$$= \frac{r}{\Delta t} \qquad (3\text{-}26)$$

The solar array angle is measured by a sixteen pole resolver to an accuracy that is not well known. For this application, a random measurement error of 0.1 degree standard deviation will be assumed, and is certainly pessimistic.

Reaction wheel speed is continuously monitored via the commutation electronics that powers the wheel. Like array measurement, its accuracy is poorly known as it was not originally intended to be included as an input to the on-orbit controller. The reaction wheel was modeled as a first-order process that satisfies the following differential equation

$$\dot{h} = -\frac{1}{\tau_w} h - \frac{K_w}{\tau_w} V_c(t) + w(t) \qquad (3\text{-}27)$$

Where K_w = 75 in.-lb-s/V, τ_w = 600 seconds, and w(t) is a white noise of spectral intensity q. The sample data representation of Eq. (3-27) for a 2-Hz rate is

$$h_{i+1} = ah_i + bV_i + gw_i \qquad (3\text{-}28)$$

where

$$a = e^{-\frac{\Delta T}{\tau w}} = 0.99917$$

$$b = -\frac{K_w}{\tau_w}\int_0^{\Delta T} e^{-\frac{\zeta}{\tau w}}\, d\zeta = -0.06247$$

$$g = \int_0^{\Delta T} e^{-\frac{\zeta}{\tau w}}\, d\zeta = 0.4998$$

w_i is a white Gaussian random sequence of variance q_k

$$g^2 q_k = q\int_0^{\Delta T} e^{-\frac{2\zeta}{\tau w}}\, d\zeta$$

$$q_k = 2q$$

The wheel measurement is modeled by

$$y_i = h_i + n_i \qquad E[n_i] = 0$$

$$E[n_i n_j] = r\delta_{ij} \tag{3-29}$$

A Kalman filter may be specified for the wheel speed according to Eq. (3-8) through (3-11). As time proceeds, the estimation error covariance and filter gains reach steady-state values that have closed form solutions, and the gain is only a function of the ratio of process to measurement noise. The steady-state Kalman gain is

$$k_{ss} = \frac{(a^2 - 1) + g^2\rho + \sqrt{[(1 - a^2) - g^2\rho]^2 + 4g^2\rho}}{(a^2 + 1) + g^2\rho + \sqrt{[(1 - a^2) - g^2\rho]^2 + 4g^2\rho}} \tag{3-30}$$

where

$$\rho = q_k/r$$

For a fixed estimator gain, the mean estimator error, e_i, decays according to the following first-order difference equation

$$e_{i+1} = (1 - k)ae_i \tag{3-31}$$

Table 3-2 presents numerical results for the Kalman gain k, and the estimation error eigenvalue for several values of ρ.

Table 3-2. Wheel-speed estimation parameters.

ρ	Gain	Eigenvalue
0.001	0.001488	0.9843
0.01	0.0480	0.9512
0.1	0.1454	0.8539
1	0.3899	0.6096
10	0.7654	0.2344
100	0.9629	0.03709
1000	0.9960	0.00397

Given that little is known about the measurement quality, a filter will be chosen in line with the reasoning presented earlier in this section, that is, as slow as possible but still faster than the controlled plant poles. For the reaction wheel, a process to measurement noise of one to one is suitable.

The dominant disturbance on the reaction wheel is a motor cogging torque. In the manufacturer's System Analysis Report (1976), the cogging torque is modeled as

$$T = 0.25 \sin \left[96 \int \omega_{Fw} \, dt \right] \text{ in.-oz} \tag{3-32}$$

where ω_{Fw} is the reaction wheel speed in rad/s. Cogging torque will be modeled as a white random sequence with a standard deviation that matches the rms value of the sinusoid, which is 0.011 in.-lb. With the process noise specified, the measurement noise is then set to an rms value of 0.011 in.-lb-s.

All unmodeled internal and external disturbances and higher-order dynamics such as flexible modes are lumped together and modeled as two white Gaussian sequences acting externally on the solar array and satellite body. The dominant body disturbances about the pitch axis are the array cogging torques, and approximately 1 percent of the torque generated by a large telescope scanning in the roll plane that inertially couples into the pitch axis.

The combined rms of the body disturbances is 0.7 in.-lb and is chosen as the value of that process noise. Major solar array disturbances include cogging torque, flexing of the array, and low frequency external torques, predominately gravity gradiant effect. High-frequency array disturbances are not as well documented as body internal effects, so selecting a process noise is not as clear. A torque range of 1 to 10 in.-lb is reasonable for filter synthesis, and will be varied with the estimator objectives discussed earlier.

3.2.3 Evaluation and Results

Given that a number of measurement options exist, specifying an attitude filter is not as straightforward as specifying an optimal controller. In addition, it is useful to consider suboptimal filter structures such as artificially isolating certain states for the purposes of reducing computation requirements, or to eliminate undesirable cross-coupling of modes.

The questions to be addressed include the following. What filter structure makes sense for this application? What is a good choice of measurements? Do filter gains reach steady state fast enough to justify a fixed gain estimator, or is the additional computational burden of time varying gains necessary?

Answering these questions will be done by assembling appropriate stochastic model elements as described in Section 3.2.2, and propagating the estimation error covariance and Kalman gain equations, Eq. (3-9), (3-10), and (3-11).

Should steady-state gains result, the estimation error eigenvalues indicate whether or not the filter is fast enough to not interfere with the desired closed-loop response. Estimation error is defined to be

$$\underline{e}_i = \hat{\underline{x}}_i - \underline{x}_i \tag{3-33}$$

Substituting Eq. (3-6), (3-8), and (3-10) into Eq. (3-33) and taking the expectation, the mean estimation error propagates according to

$$E[\underline{e}_{i+1}] = (I - KH)\Phi E[\underline{e}_i] \tag{3-34}$$

The eigenvalues of $[(I - KH)\Phi]$ determine the speed of error decay.

Because the amount of data generated by covariance analysis is voluminous, general results and conclusions are first presented followed by numerical results of certain interesting cases.

One initial result is that the system defined in Appendix A is not completely observable. A definition of observability is that given a linear system such as

$$\underline{x}_{i+1} = \Phi\underline{x}_i + \Lambda\underline{u}_i$$

$$\underline{y}_i = H\underline{x}_i$$

and knowing a finite sequence of output and control vectors, y_1, y_2, ... y_n, u_1, u_2, ..., u_n, it is possible to calculate the initial state, $\underline{x}_0$. This condition is violated on the integral state, x_1, since it cannot be measured and knowing inputs does not allow estimation of the initial condition. As a result, the estimation error covariance of the state is not

reduced from its initial value, but grows slowly as the system covariance propagates. However, unobservability is not a real constraint because the purpose of the integral state is to sum attitude errors, so the "open-loop" estimate derived by integrating the attitude is sufficient.

After considering all of the external measurement options discussed in Section 3.2.2, the use of star mapper attitude measurements only at 2 Hz and an isolated estimator for wheel speed is the proposed filter structure. Numerical values of process and measurement noise are

$$Q = \begin{bmatrix} 0.54 & 0 & 0 \\ 0 & 1.0 & 0 \\ 0 & 0 & 0.000121 \end{bmatrix} (\text{in.-lb})^2$$

$$R = \begin{bmatrix} (12.56 \text{ arc-sec})^2 & 0 & 0 \\ 0 & (0.1 \text{ deg})^2 & 0 \\ 0 & 0 & (0.011 \text{ in.-lb})^2 \end{bmatrix}$$

Within 30 seconds, the full-order covariance matrix converged, with the exception of the integral state, to the following steady-state values of estimation error standard deviation;

Pitch	0.0033 deg	(12 arc-sec)
Pitch Rate	0.015 deg/s	
Array	0.066 deg	
Array Rate	0.059 deg/s	
Wheel	0.0065 in.-lb-s	

Estimation error eigenvalues are plotted in Figure 3-11.

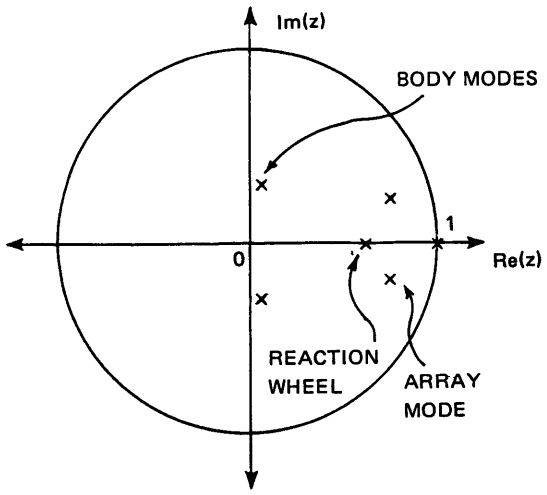

Figure 3-11. Full-order filter eigenvalues, star mapper.

The Kalman gain matrix for the full-order filter is, in steady state

$$K = \begin{bmatrix} 0.2303 & 0.190 \times 10^{-3} & -0.563 \times 10^{-8} \\ 0.9128 & -0.584 \times 10^{-3} & 0.103 \times 10^{-7} \\ 1.9899 & -0.213 \times 10^{-2} & 0.147 \times 10^{-6} \\ -0.4798 & 0.4347 & -0.983 \times 10^{-8} \\ -1.7484 & 0.2477 & -0.146 \times 10^{-6} \\ 0.335 \times 10^{-3} & -0.390 \times 10^{-6} & 0.3899 \end{bmatrix}$$

Note that from the steady state gains, pitch and pitch rate are estimated almost entirely by star mapper measurements, array and array rate by combinations of star mapper and array measurements, and wheel momentum almost entirely by its measurements. It is clear that the implementation of this filter would logically isolate the wheel from the rest of the system, and that other near zero gains could be set to zero as follows

$$K = \begin{bmatrix} 0.2303 & 0 & 0 \\ 0.9128 & 0 & 0 \\ 1.9899 & 0 & 0 \\ -0.4798 & 0.4347 & 0 \\ -1.7484 & 0.2477 & 0 \\ 0 & 0 & 0.3899 \end{bmatrix}$$

From the eigenvalue plot, it can be seen that this proposed filter is faster than the closed-loop modes plotted in Figure 3-1. It also turns out that the dominant filter gains settle to within 10% of their final values within the second or third iteration, so a time invariant estimator is justified.

It is reasonable to predict that if a direct measurement of rate information were available, an attitude estimator would perform better than if no rate information is available. The measurement quality required before filter improvement is useful is not obvious, but can easily be experimented with. Two approaches to obtaining rate information are applicable in this case, from gyros or from preprocessed star mapper measurements. It may be possible to use less accurate, and consequently less expensive, rate gyros than currently exist on the spacecraft. The effects of varying qualities of direct rate information, such as obtained from gyros, on an estimator for pitch and array states only are presented in Table 3-3. Filter performance to a derived rate estimate by back-differencing two 0.1-second star mapper measurements with measurement and process correlations as discussed in the previous section is also listed. Process noise remains unchanged.

Steady-state estimation error eigenvalues for the filters that produced these results are plotted in Figure 3-12.

Judging from the variances listed in Table 3-3 it seems that the best rate information, of a quality which is easily superceded by the current gyros, should be used because of the good reduction in estimation error. However, the eigenvalues of this filter, Case 4 in Figure 3-12

Table 3-3. Star mapper filter variances with direct rate information.

Rate Measurement		Steady-State Error Variances			
Case	Noise $(deg/s)^2$	Pitch $(deg)^2$	Pitch Rate $(deg/s)^2$	Array $(deg)^2$	Array Rate (deg/s)
1	∞ (no measurement)	$(0.00333)^2$	$(0.0152)^2$	$(0.0659)^2$	$(0.0589)^2$
2	$(0.1)^2$	$(0.00332)^2$	$(0.0151)^2$	$(0.0659)^2$	$(0.0588)^2$
3	$(0.01)^2$	$(0.00282)^2$	$(0.00826)^2$	$(0.0659)^2$	$(0.0575)^2$
4	$(0.001)^2$	$(0.00126)^2$	$(0.000997)^2$	$(0.0659)^2$	$(0.0569)^2$
5	back difference $\approx(0.05)^2$	$(0.00270)^2$	$(0.0147)^2$	$(0.0659)^2$	$(0.0588)^2$

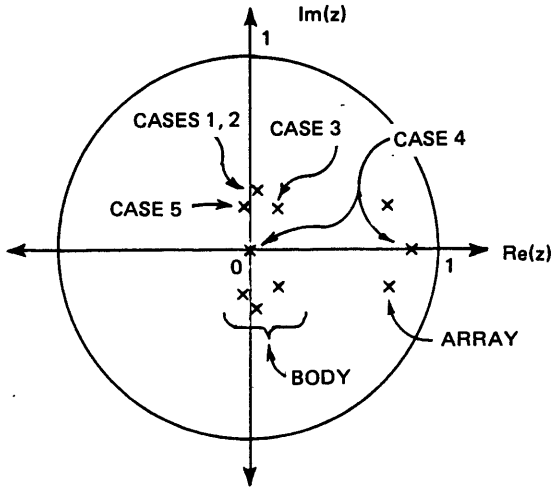

Figure 3-12. Star mapper filter eigenvalues with direct rate information.

illustrate that error statistics alone are not good performance measures. Good rate measurements allow a near dead-beat rate error response, but the optimal filter slows down the attitude estimate to an unacceptable level. Back differenced rate measurements offer an attractive candidate for enhancing filter performance with only a slight computational burden. The improvement, however, is also slight, and it is not clear that any

better performance is required. Star sensor noise was assumed to be that of the dimmest usable stars with an rms error of 12.6 arc-sec, and filter performance appears to be adequate. Since estimation accuracy is so closely tied to sensor accuracy, the presence of brighter stars stands to reduce estimation errors in line with Table 3-1, and minor improvements with rate information have even less to offer.

Incorporating gyro measurements are considered in a similar manner. Two filter structure options are considered; using attitude increments only at 2 Hz, or including a rate measurement derived by differencing two attitude increments 0.1 second apart.

The gyro based attitude filter does not ever reach a steady state because gyro errors are modeled as a random walk plus uncorrelated errors. After the initial covariance matrix is reshaped with the first few seconds of data, the pitch variance closely followed a random walk increasing $(0.013 \text{ arc-sec})^2$ per iteration. However, the variances of pitch rate and array states did stabilize in only a few seconds, as did all of the elements of the gain matrix. Table 3-4 presents the results of using gyro measurements in a four-state filter estimating body and array modes, and stopping the filter at 15 seconds. Process noise is unchanged from previous cases.

Table 3-4. Gyro filter variances.

Case	Measurements	Pitch $(\text{arc-sec})^2$	Pitch Rate $(\text{arc-sec/s})^2$	Array $(\text{deg})^2$	Array Rate $(\text{deg/s})^2$
1	Attitude	$(0.0735)^2$	$(7.75)^2$	$(0.0659)^2$	$(0.0569)^2$
2	Attitude and Rate	$(0.0612)^2$	$(0.0406)^2$	$(0.0659)^2$	$(0.0569)^2$

Estimation error eigenvalues are plotted in Figure 3-13 for these two cases.

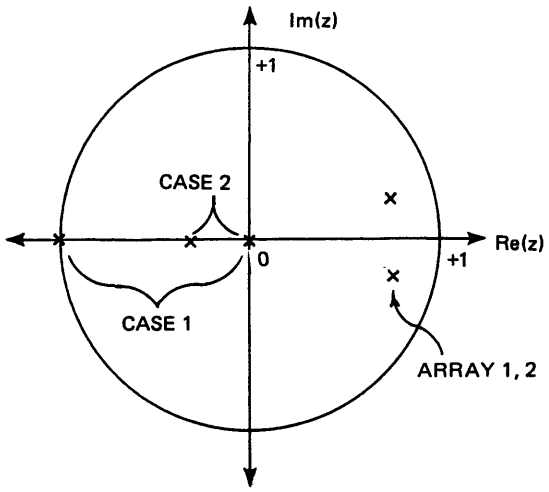

Figure 3-13. Gyro filter eigenvalues.

From the error covariances listed in Table 3-4 it is clear that gyro measurements can allow much faster filtering and still produce vastly higher quality estimates than any of the measurement combinations relying on star mapper attitude information. Although attitude covariance increases linearly with time, over the time span the gyro's spectral density is valid, which is under 1000 seconds, it is clear that the error will not reach the worst-case error resulting from using a star mapper.

Estimator performance is significantly enhanced by using a direct rate measurement. If attitude increments alone are measured at 2 Hz, the rate error eigenvalue is placed at z = -0.9899 resulting in a curious slow exponential decay with alternating signs that is unique to discrete time systems. Incorporating back-differenced rate information shifts that pole to z = 0.3355, moving the decay time constant lower than all closed-loop plant time constants.

Including the reaction wheel state in the model with gyro attitude and rate measurements illustrates an interesting characteristic of linear estimation. All other filter schemes, when wheel momentum was added to the model, calculated the same optimal gain as was presented for the wheel alone in Eq. (3-30) and set the gains on other measurements essentially to zero for that state. With pitch and pitch rate both accurately measured, the Kalman gain matrix, at t = 15 seconds, for the five state model, ignoring the integral of attitude error is

$$K = \begin{array}{c} \\ \text{Pitch} \\ \text{Pitch Rate} \\ \text{Array} \\ \text{Array Rate} \\ \text{Wheel} \end{array} \begin{array}{c} \begin{array}{cccc} \text{Pitch} & \text{Pitch Rate} & \text{Array} & \text{Wheel} \end{array} \\ \begin{bmatrix} 0.6544 & 0.09600 & 0.2 \times 10^{-10} & -0.2 \times 10^{-7} \\ 0.9013 & 0.8607 & -0.1 \times 10^{-8} & -0.2 \times 10^{-7} \\ -0.3328 & -0.06471 & 0.4343 & 0.5 \times 10^{-8} \\ -0.7260 & -0.8412 & 0.2457 & 0.1 \times 10^{-7} \\ -212.9 & 59.15 & 0.2 \times 10^{-6} & 0.3899 \end{bmatrix} \end{array} \begin{array}{l} \text{Measurement} \\ \\ \text{Estimate} \\ \text{Pitch} \\ \text{Pitch Rate} \\ \text{Array} \\ \text{Array Rate} \\ \text{Wheel} \end{array}$$

Knowing pitch and its rate accurately allows the estimator to "think" it has enough sensitivity to improve the wheel momentum estimate through the weak coupling introduced by the long exponential decay model assumed for the wheel. Implicit in the theory of linear estimation is the assumption of perfect modeling, and this case shows a potential problem from such an assumption. Since the reaction wheel is actually very complex, with inner compensation loops and the full range of dynamics of an electromechanical system, a first-order model, while adequate for modeling its effect as an actuator, is not suitable for providing an accurate weak correlation suitable for exploiting in an estimator to the degree the calculated gains indicate. A number of solutions are available, the simplest being to merely remove the wheel from the model and run a separate estimation loop for it. Other possibilities include increasing the order of the gyro model, or proportionally reducing the wheel process and measurement noise until the direct wheel measurement becomes the dominant input to wheel estimate as engineering judgement indicates it should be.

It is clear that gyro data, either from the existing rate integrating gyros, or in the form of direct rate measurements with star mapper attitude measurements will produce superior estimation results than can be had if star mapper attitude only measurements drive the filter. The justificaton for recommending that the filter should rely on 2-Hz star mapper measurements as its only inertial attitude input is that such a structure produces adequate results. The additional cost

and computational burden introduced by requiring gyros or deriving direct rate information does not seem necessary. In addition, the proposed filter has been evaluated under pessimistic assumptions. Star mapper error will almost always be lower, and the disturbance model is definitely severe. All further simulation and analysis will use this proposed filter.

3.3 Combined Filter/Controller

With a Kalman filter to estimate the state, the optimal feedback gains calculated under the assumptions of perfect state knowledge are used to determine control commands to the reaction wheel and solar array drive. Figure 3-14 diagrams the complete loop and illustrates the mix of continuous and discrete time processes.

3.3.1 Deterministic Response

A useful evaluation is to repeat the transient responses of Section 3.1.4 with no random inputs, since this also illustrates the mean trajectory of the real process. Figure 3-15 plots the response to an initial pitch error of 1 degree and no initial estimation error. As expected, response is identical to that of Figure 3-1. The estimator is able to track the state perfectly. If the initial pitch estimate is set to zero, the response changes as can be seen in Figure 3-16. Although estimation errors decay fast; large controls are commanded during the error transient, which would saturate both actuator input limits. This is a severe test, however, since the optimal estimator gain matrix for a high initial uncertainty has a significantly different structure than the steady-state gains based on an accurate previous knowledge of state. Time varying filter gains would diminish the effect of large initial errors, but a simpler approach for implementation would be to run the estimator for a few seconds before allowing control commands to be issued instead of turning both on at once.

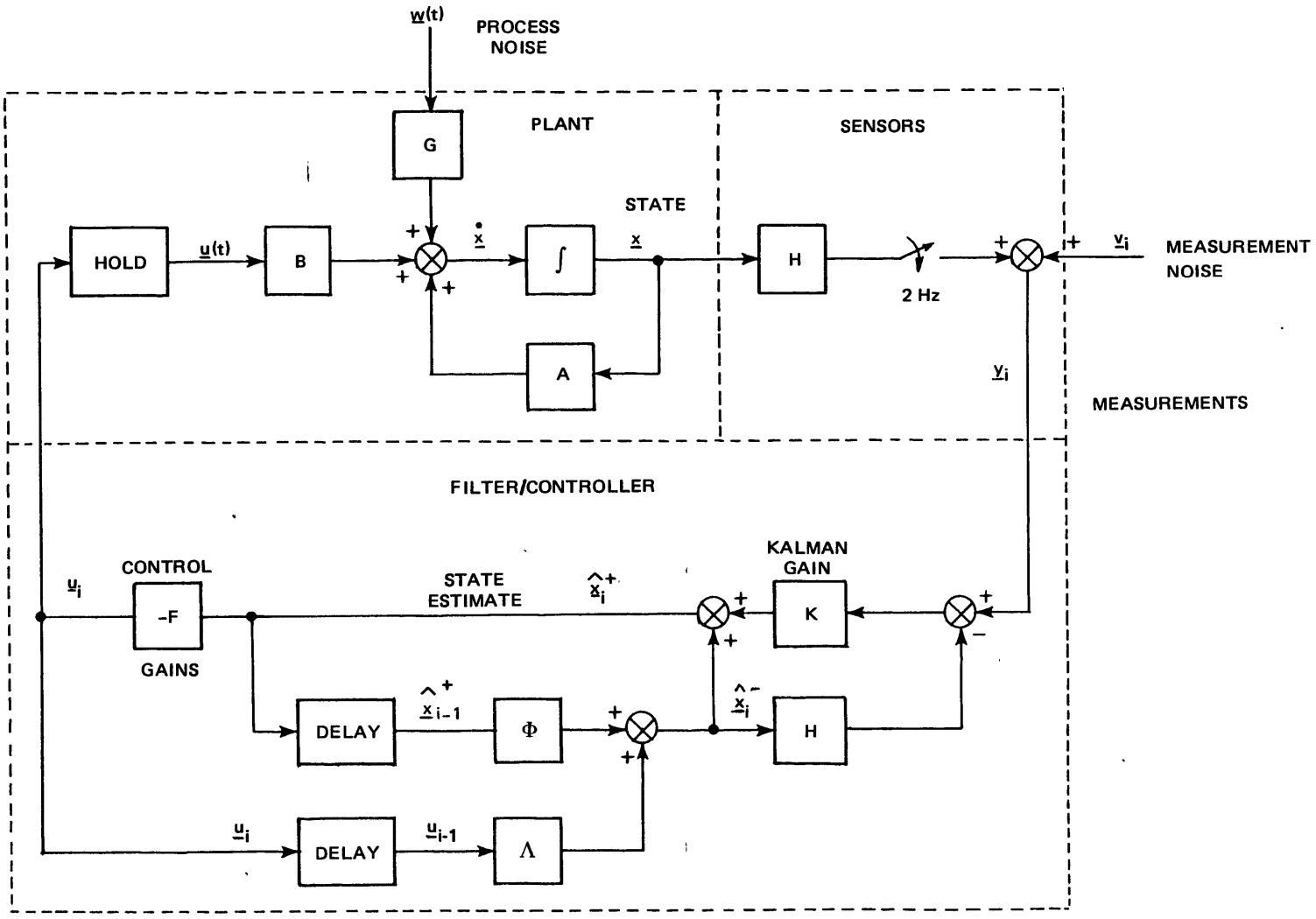

Figure 3-14. Closed-loop control.

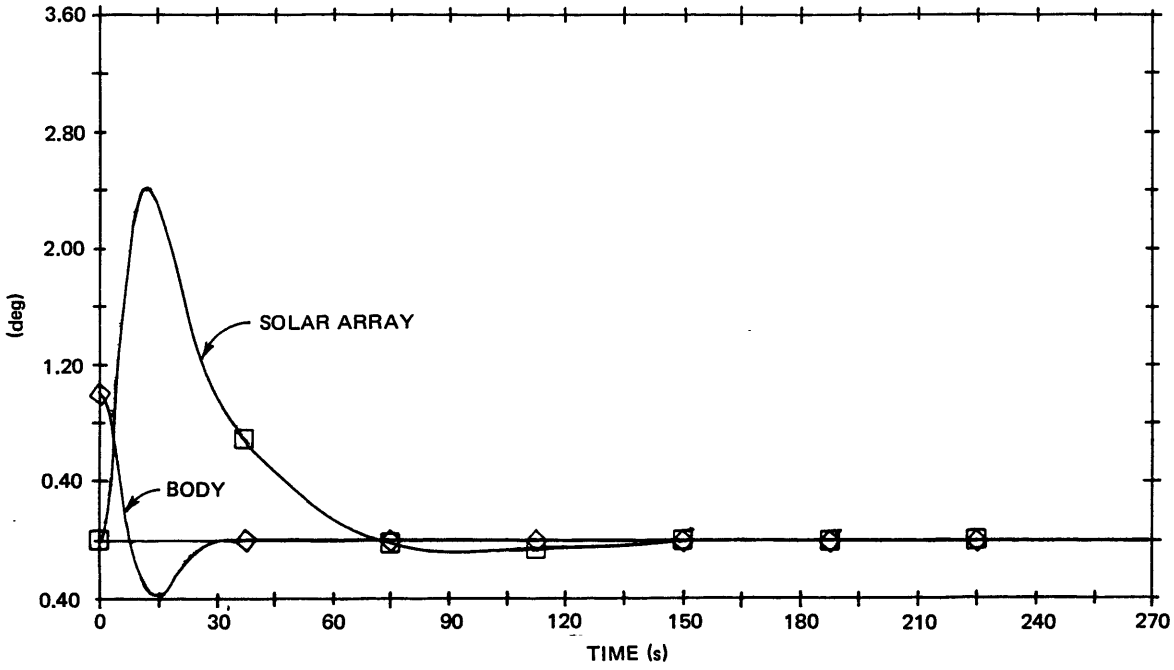

Figure 3-15. 2-Hz filter/controller; no estimation error, no noise.

3.3.2 Stochastic Response

The ability to easily evaluate effects of random disturbances is a powerful feature of linear system theory, and is important for this application. At sample times, the process diagrammed in Figure 3-14 may be represented by a 2n order set of difference equations, where n is the order of the state vector. Changing variables to use estimation error as a partition of the state, these equations may be written as

$$\begin{bmatrix} \underline{x}_{i+1} \\ \hline \underline{e}_{i+1} \end{bmatrix} = \begin{bmatrix} \Phi - \Lambda F & -\Lambda F \\ \hline 0 & (I - KH)\Phi \end{bmatrix} \begin{bmatrix} \underline{x}_i \\ \underline{e}_i \end{bmatrix} + \begin{bmatrix} \Gamma & 0 \\ \hline (KH - I)\Gamma & K \end{bmatrix} \begin{bmatrix} \underline{w}_i \\ \hline \underline{v}_{i+1} \end{bmatrix} \quad (3\text{-}35)$$

where

$$\underline{e}_i = \hat{\underline{x}}_i - \underline{x}_i$$

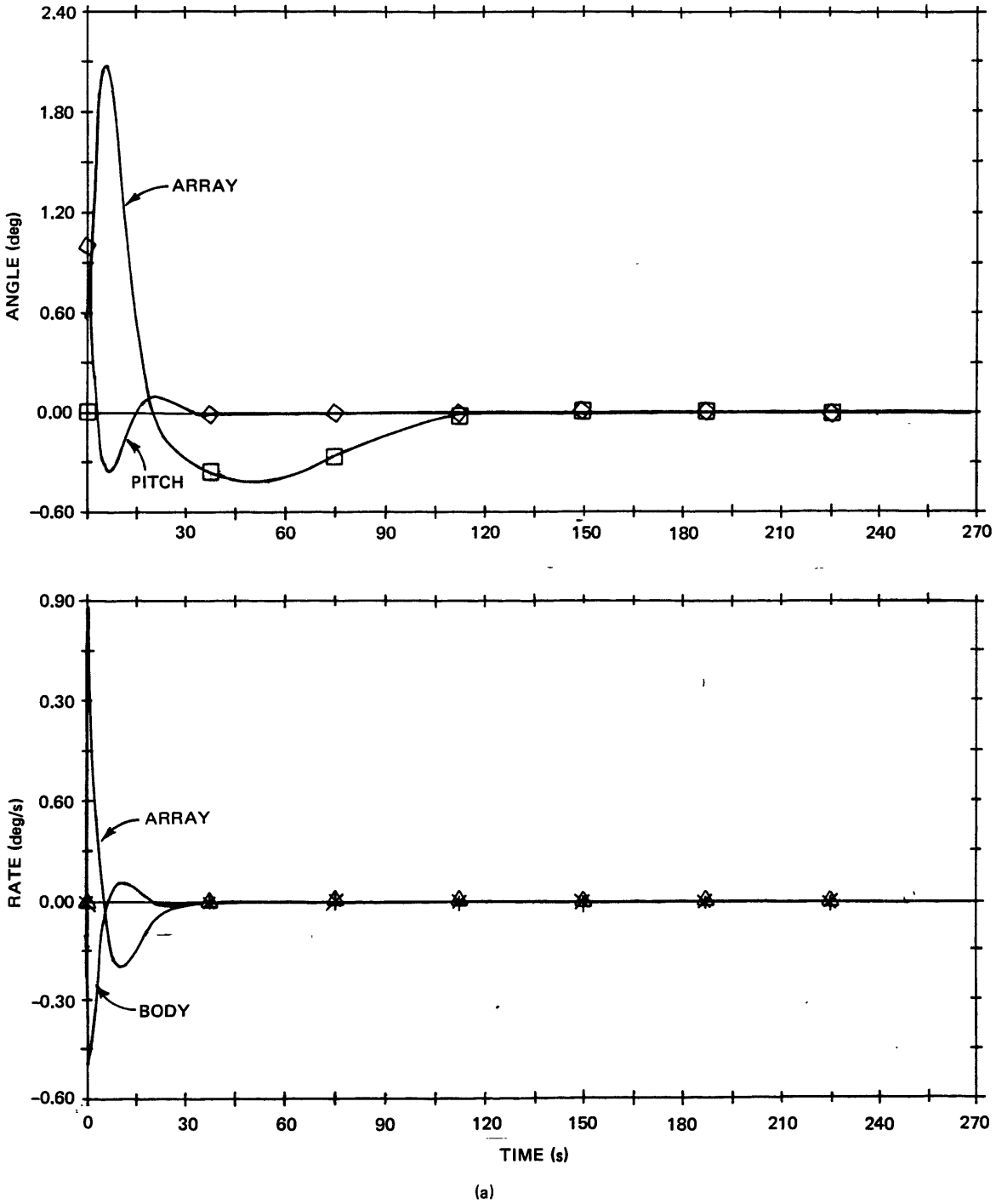

Figure 3-16. 2-Hz filter/controller; initial estimation error, no noise.

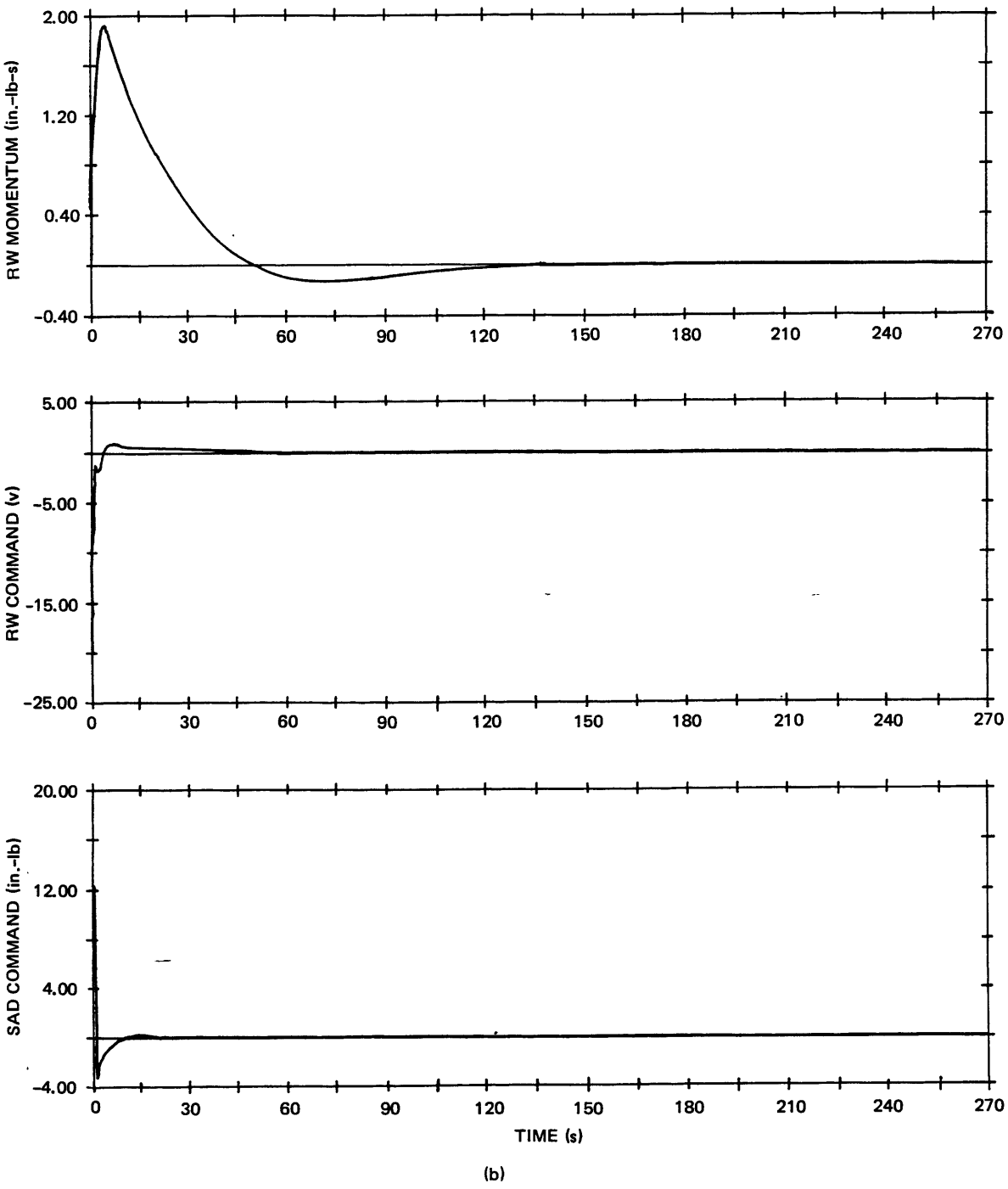

Figure 3-16. 2-Hz filter/controller; initial estimation error, no noise. (Cont.)

The zero partition of the homogeneous term in Eq. (3-35) illustrates the classic result of full-order estimated state feedback that the eigenvalues of the closed-loop system are the eigenvalues of $[\Phi - \Lambda F]$, identical to the deteministic state feedback case and the eigenvalues of $[(I - KH)\Phi]$, estimate error decay. The timing discrepancy in the combined driving vector is a result of the fact a Kalman filter uses measurements immediately. Since $\underline{w}_i$ and $\underline{v}_i$ are modeled as uncorrelated sequences, it is as matter of notation and not of physical significance. Equation (3-35) represents a linear system driven by an uncorrelated process, and the covariance propagation is given by

$$P'_{i+1} = \Phi' P'_i \Phi'^T + \Gamma' Q' \Gamma'^T \qquad (3\text{-}36)$$

where

$$P' = E\left\{\begin{bmatrix} \underline{x}_i \\ \underline{e}_i \end{bmatrix}\begin{bmatrix} \underline{x}_i^T & \underline{e}_i^T \end{bmatrix}\right\}$$

$$\Phi' = \left[\begin{array}{c|c} \Phi - \Lambda F & -\Lambda F \\ \hline 0 & (I - KH)\Phi \end{array}\right]$$

$$\Gamma' = \left[\begin{array}{c|c} \Gamma & 0 \\ \hline (KH - I)\Gamma & K \end{array}\right]$$

$$Q'_i = E\left\{\begin{bmatrix} \underline{w}_i \\ \hline \underline{v}_{i+1} \end{bmatrix}\begin{bmatrix} \underline{w}_j^T & \underline{v}_{j+1}^T \end{bmatrix}\right\} = \left[\begin{array}{c|c} Q & 0 \\ \hline 0 & R \end{array}\right]\delta_{ij}$$

An initially obvious choice for Q and R is the same value used in the filter design. There are, however, some doubts on the validity of the process noise for predicting closed-loop errors. Actual disturbances acting on the spacecraft are all nearly pure sinusoids, and the

high-frequency internal disturbances that have the largest magnitudes cannot change total system momentum. An uncorrelated external disturbing torque of similar intensity, while a useful approximation for filter synthesis, will cause the mean-squared value of total system momentum to increase with time, which is a significant difference from physical reality.

Uncorrelated sensor noise is a close approximation to real uncertainties, and since the system is linear, the contribution to pointing error from sensor noise alone can be calculated. Furthermore, sensor noise in no way affects total angular momentum so avoids the physical problems associated with external torque noise. Table 3-5 lists the root mean square pitch and array errors for several combinations of measurement noises and intensities. Filter gains are the reduced order gains specified in Section 3.2.3.

Table 3-5. Steady-state rms errors under optimal control.

Measurement Noise Intensities			rms Pointing Errors	
Pitch $(\text{arc-sec})^2$	Array $(\text{deg})^2$	Wheel $(\text{in.-lb-s})^2$	Pitch (arc-sec)	Array (deg)
$(0.32)^2$	0	0	0.148	0.00008
$(12.56)^2$	0	0	5.81	0.00178
0	$(0.1)^2$	0	6.37	0.0167
0	0	$(0.011)^2$	0.012	0.00005
$(0.32)^2$	$(0.1)^2$	$(0.011)^2$	6.37	0.0167
$(12.56)^2$	$(0.1)^2$	$(0.011)^2$	8.62	0.0170

The lower case of pitch measurement noise corresponds to a star of magnitude 1 in the field of view, while the higher case represents the dimmest usable star of 6^{th} magnitude. From these results it is clear that star mapper noise will not contribute significantly to pointing when a bright star is available. Most of the pointing error is a result of the noisy array measurement.

It is interesting to calculate the effect of similar noises on the present control law. The estimator will not be changed, since body and array rates must be derived some way, but instead of using an optimal feedback gain matrix the sparce matrix introduced in Section 3.1 will be used. Table 3-6 contains the results.

Table 3-6. Steady-state rms errors under present control law.

Measurement Noise Intensities			rms Pointing Errors	
Pitch $(\text{arc-sec})^2$	Array_2 $(\text{deg})^2$	Wheel $(\text{in.-lb-s})^2$	Pitch (arc-sec)	Array (deg)
$(12.56)^2$	0	0	6.42	0.0028
0	$(0.1)^2$	0	117.5	0.0609
0	0	$(0.011)^2$	0.00128	0.178×10^{-6}
$(12.56)^2$	$(0.1)^2$	$(0.011)^2$	117.7	0.0609

Notice that sensitivity to star mapper noise is increased somewhat. Array noise causes a severe problem in this case, driving body pointing out of its 36 arc-sec limit if in fact, the noise model is good. Since the full state feedback approximation to array control is not rigorously correct these results should be interpreted only in comparison to the results of Table 3-5.

The conclusion drawn from covariance analysis is that the proposed optimal controller shows less sensitivity to estimation errors than the present feedback gains. In addition, under optimal control and worst case assumptions, measurement noise alone will not drive the pointing error out of limits, so the feasibility of this scheme is not invalidated. The effects of the many but well known nonlinear torque disturbances is the topic of the next chapter.

CHAPTER 4

EVALUATIONS

Linear theory provides a powerful method to synthesize a control system and evaluate its response to random disturbances that are either "white" or modeled by a linear network driven by an uncorrelated process. For this case, many important disturbances fit neither into the category of linear dynamics, includable in the model, or the special class of random disturbances mentioned. Without convenient rigorous mathematical tools to apply, numerical simulation provides a useful although case-specific means to analyze nonlinearities.

4.1 Disturbances

Three important classes of disturbances must be considered; relatively strong high frequency internal torques, low frequency weak external torques, and inertial cross-coupling. Almost no purely random torque disturbance exists.

4.1.1 Internal Torques

Lumped into this category are the effects of all on-board mechanisms that disturb attitude. Only very small amounts of angular momentum can be stored in any of these devices, so none can cause a significant rate drift. However, several are strong, and can cause large cyclic attitude errors. For the pitch axis, major disturbances are solar array drive cogging and, through misalignments and inertial coupling, about 1 percent of the torque generated about the roll axis by a scanning telescope.

The array drive is a 96-pole direct drive motor that exhibits noticeable cogging effects at its nominal rate of one revolution per orbit. Both viscous and dry friction are also present but initially neglected. Actual motor torque is given by

$$T_{SAD} = K_T(V_a - K_b\dot{\theta}) + \underbrace{0.18 \sin(96\theta)}_{\text{cogging torque}} - \underbrace{1.25 \left\{\frac{|\dot{\theta}|}{\dot{\theta}}\right\}}_{\substack{\text{coloumb} \\ \text{friction}}} \text{ in.-lb} \qquad (4\text{-}1)$$

where

K_T = 0.138 in.-lb

K_b = 1.03 V-s/rad

If the control law developed in Chapter 3 operates, with appropriate scaling for K_T, directly through the real SAD motor, the response is severely degraded as shown in Figure 4-1. Note that the array rate is being driven to the desired 0.06 deg/s, but dry friction introduces a constant drag and prevents array error from being nulled. The steady-state periodic shape of the response is not exactly sinusoidal since cogging torque is spatially determined, not temporally. Peak pitch error is 0.17 degree, clearly unsatisfactory.

A number of options exist to correct the cogging problem. On the current satellites a high-gain position loop controls the array. This approach would prevent most of the attractive features of optimal control from being exploited though. New optimal gains, with high penalties on array and perhaps pitch errors, could be derived. The drawback is that the resulting high bandwidth loops require higher control activity and show greater sensitivity to estimation noise. The nonlinear nature of the cogging and coloumb torques prevent direct inclusion in the model. While a linearized model can be derived, the resulting feedback gains are time varying.

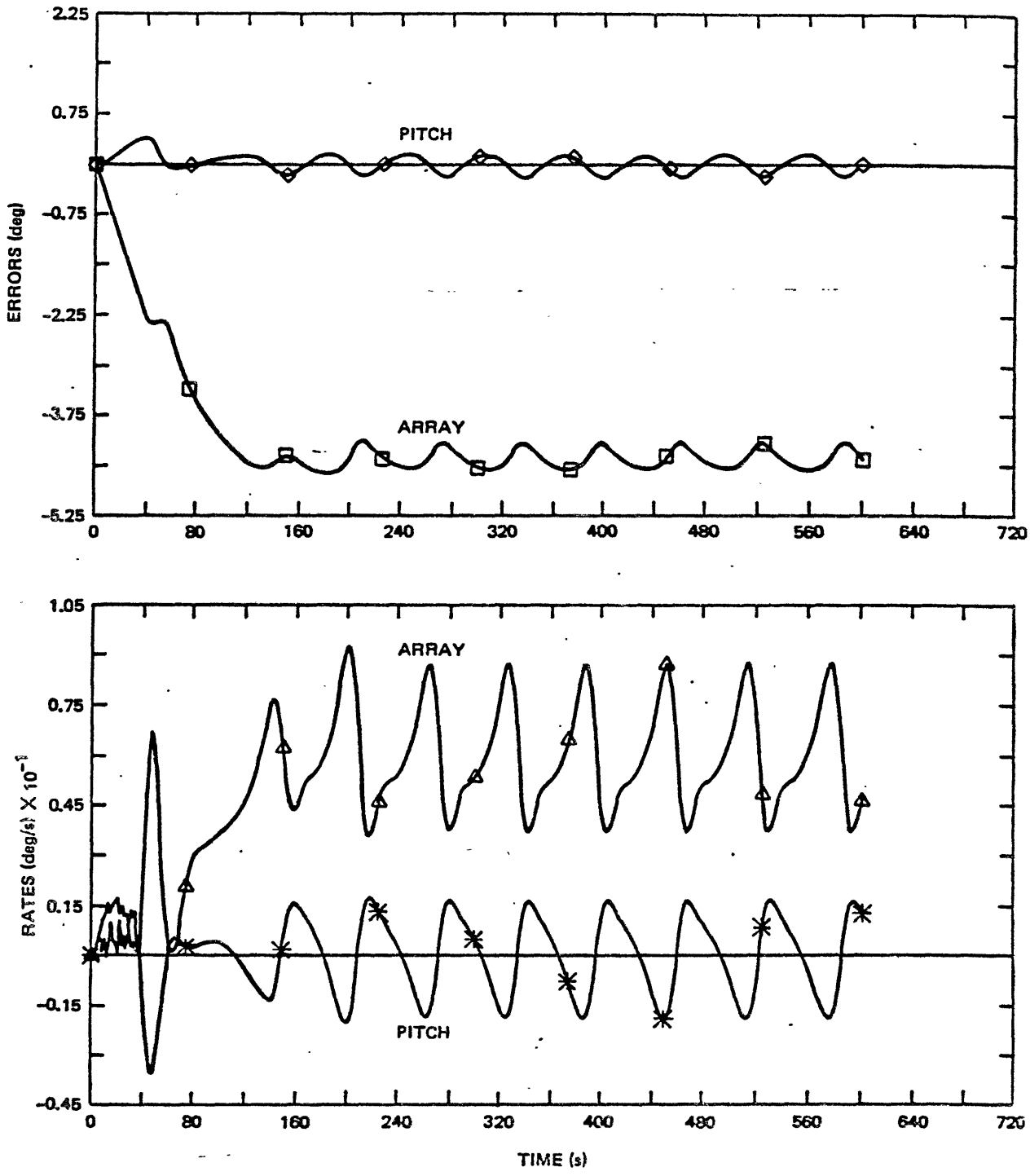

Figure 4-1. 2-Hz filter/controller; response to cogging torque.

An attractive approach for this case is to locally compensate the array drive so cogging is suppressed, but the motor "looks" like a true torque transducer to the optimal controller. From the model equations derived in Appendix A, array rate is given by

$$\dot{\theta}(t) = \int_0^t \ddot{\theta}(t)\, dt = \int_0^t \left[\frac{-1}{I_b \tau_w} h(t) - \frac{K_w}{I_b \tau_w} V_c(t) + \left(\frac{1}{I_a} + \frac{1}{I_b} \right) T_{ca}(t) \right] dt \qquad (4\text{-}2)$$

if in fact the array drive was perfect. The terms in Eq. (4-2) are all known to the controller, so Eq. (4-2) can represent a reference signal for a rate loop to track. The resulting closed loop is diagrammed in Figure 4-2.

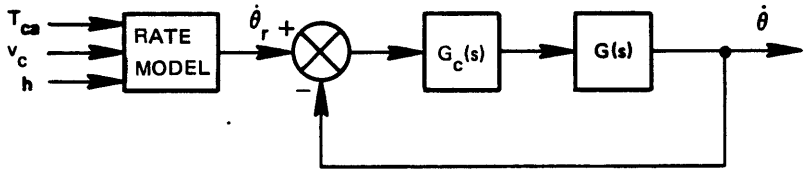

Figure 4-2. Array rate loop.

G(s) is the motor voltage to array rate transfer function, and $G_c(s)$ is a forward compensator. Appendix C develops and evaluates the loop in detail. Including array rate compensation results in an overall response as illustrated in Figure 4-3. Note that peak steady state pitch errors are 6 arcseconds, and although a steady state array error still exists, it is down to just under 0.2 degree. Plots in Appendix C also show that the rate compensator does not degrade initial condition response from the ideal case.

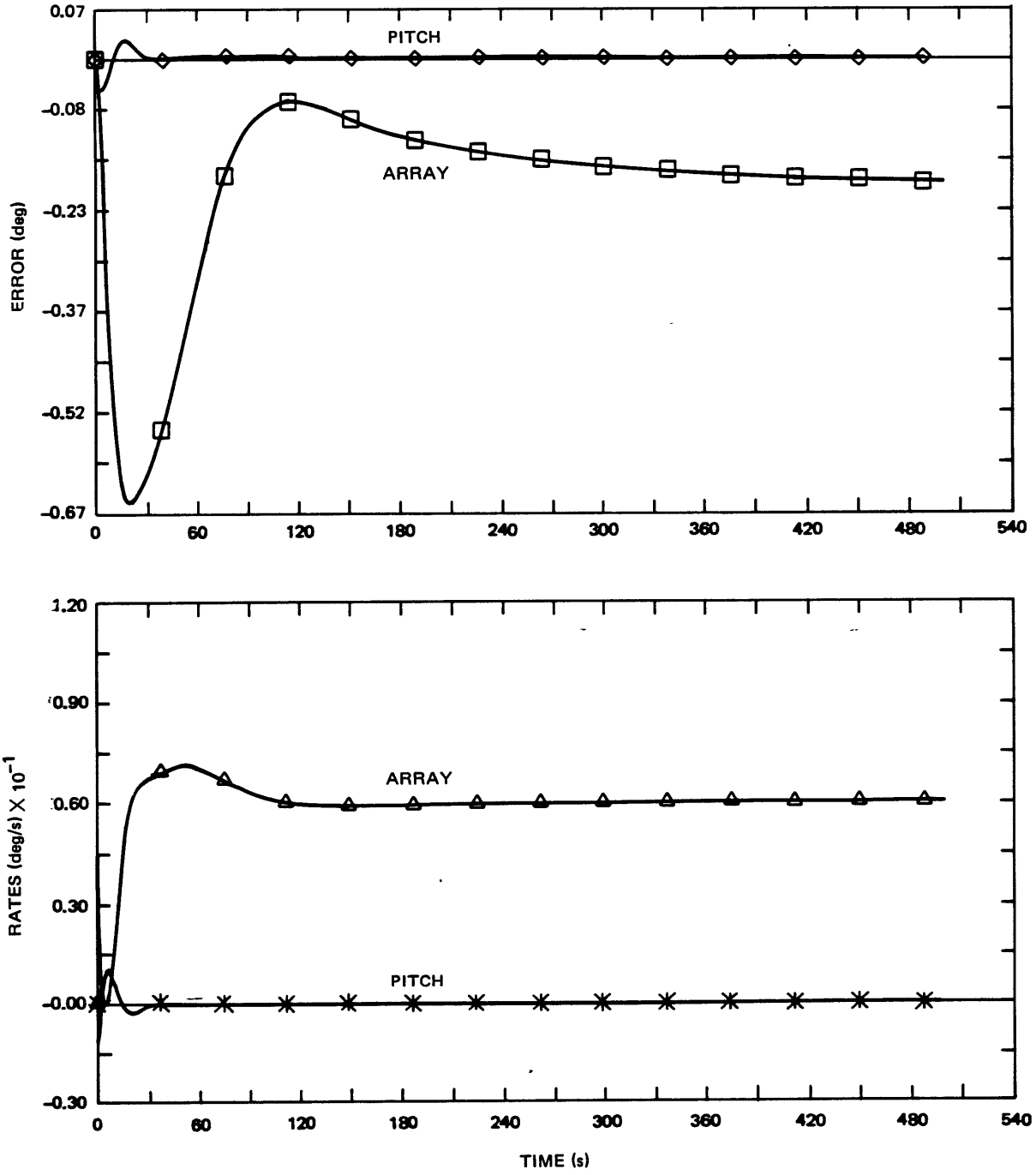

(a)

Figure 4-3. 2-Hz filter controller and SAD rate loop, response to cogging torque.

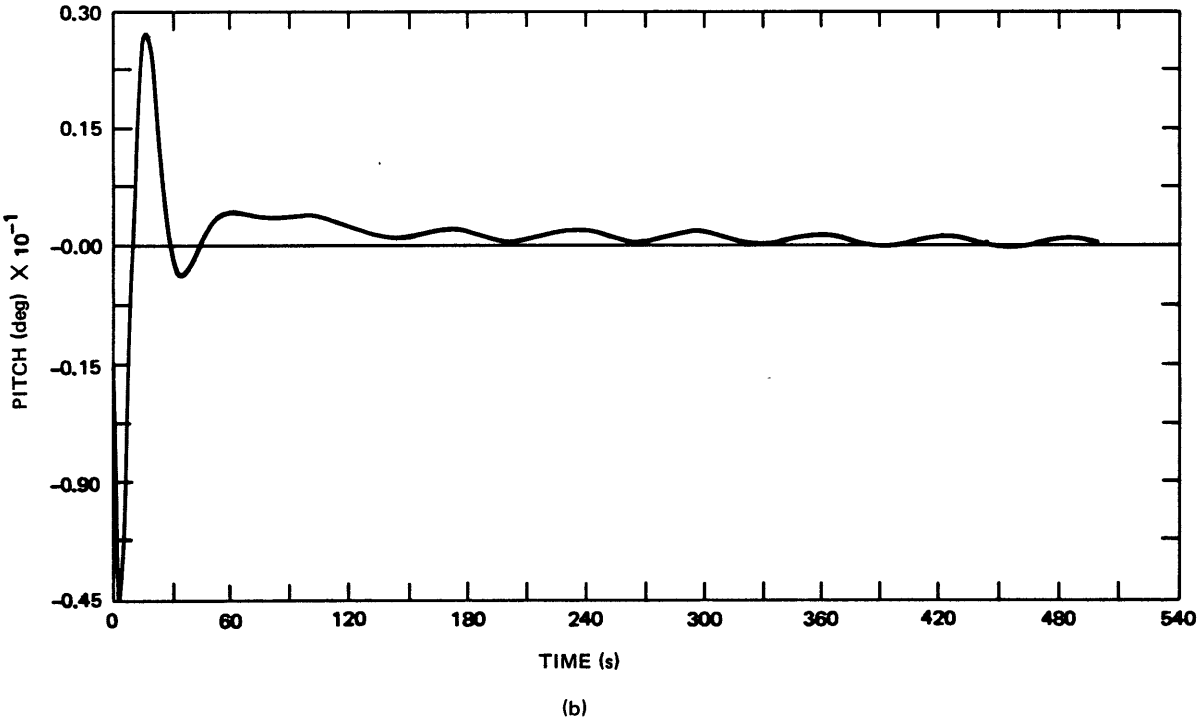

Figure 4-3. 2-Hz filter/controller and SAD rate loop, response to cogging torque (Cont.)

One might ask why similar results could not have been obtained with appropriate state augmentation and penalty weightings in the optimal framework. It is certainly possible that they could, but it is not clear how an engineer would get the insight to choose additional dynamics. With single input, single output, and a torque rejection requirement over a specific band of frequencies, the array drive presented a well posed classical control problem. In addition, the overall dimension of the control problem has not been increased by as much as state vector augmentation and optimal control would require.

The second particularly strong high frequency internal torque results from the 6-Hz scanning of a large telescope in the yaw-pitch plane. Most of the reaction torque acts against the large roll moment of inertia but about 1 percent appears on the pitch axis through inertial coupling, and is modeled by

$$T_d = (0.01)(82.1) \cos \omega t \text{ in.-lb}$$

$$\omega = 12\pi \text{ rad/s}$$

Without any control action, peak pitch deflection should be limited to 0.13 arcsecond by pitch inertia. Since 6 Hz is well over the sampling rate, a short simulation was run to see if aliasing effects were noticed. Figure 4-4 shows pitch response to scanning torque superimposed on residual cogging torque, and additional error is on the order predicted.

Cogging torque is also noticeable on the reaction wheel drive. The disturbance, transmitted equally to the wheel and satellite body, is modeled by

$$T_d = 0.016 \sin \left(96 \int_0^t \omega_{Fw} dt \right) \text{ in.-lb}$$

$$\omega_{Fw} = \text{angular velocity of wheel, rad/s}$$

Wheel speed varies over ±900 rad/s, so the cogging frequency is almost always out of the bandwidth of the control systems. At a constant wheel speed of 1 rpm, which is certainly a lower limit on the validity of the cogging model, peak pitch deflection is 0.036 arcsecond. Error magnitude falls off as the inverse square of wheel speed, so for normal operations wheel cogging effects are negligable. Wheel reversal does introduce a transient disturbance, largely from stiction, but it is possible to put a bias momentum on the pitch wheel to prevent this.

The smallest known disturbance about the pitch axis is caused by a tape recorder driver. Torque pulses appear as shown in Figure 4-5.

The pattern repeats for 60 cycles, then the order of torque signs reverses for 60 cycles. Peak deflection occurs at the center of a pulse input as the torque sign changes and is limited to 0.001 arcsecond by body inertia alone.

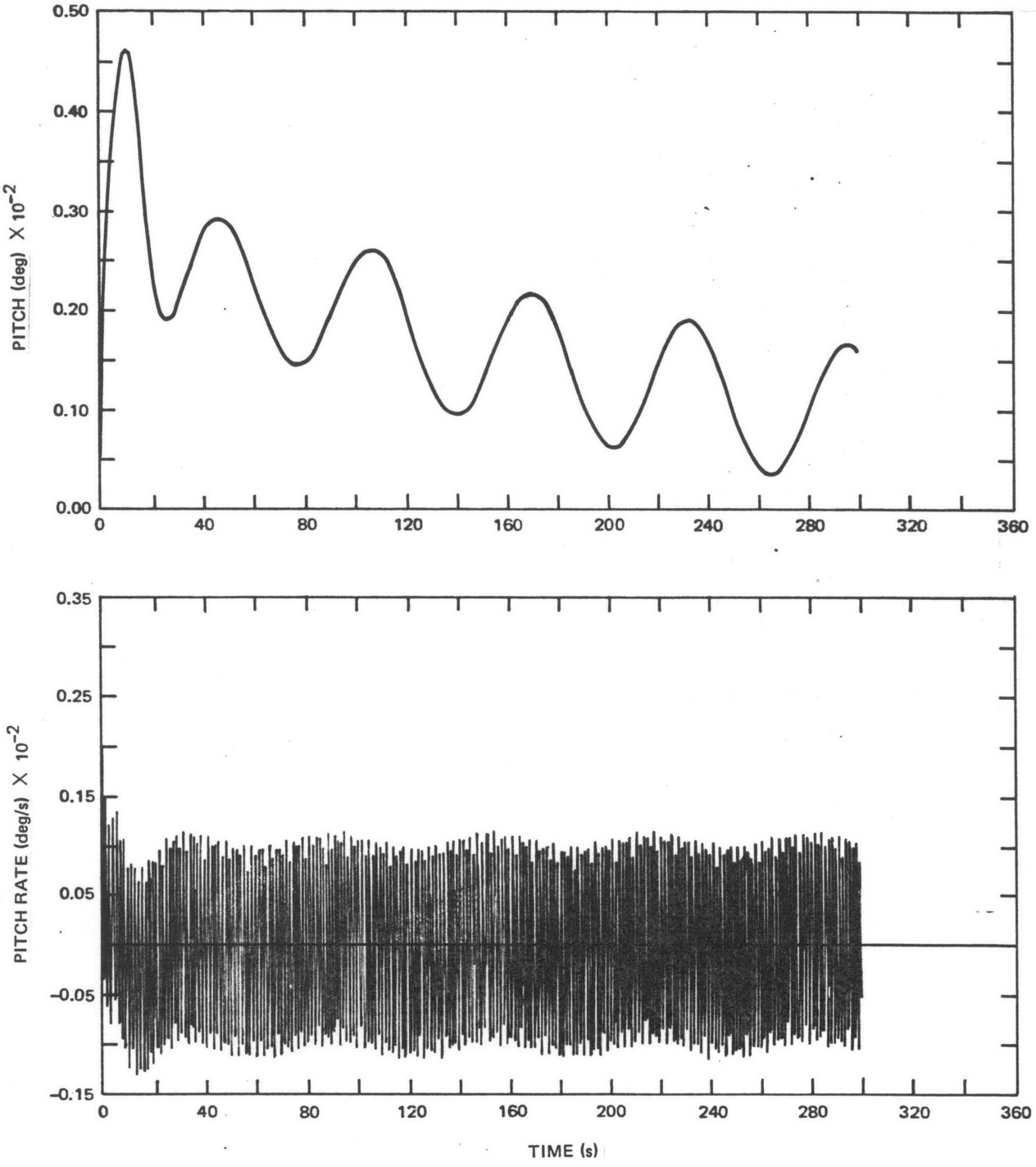

Figure 4-4. 2-Hz filter controller and SAD rate loop, response to cogging, external, and telescope scanning torques.

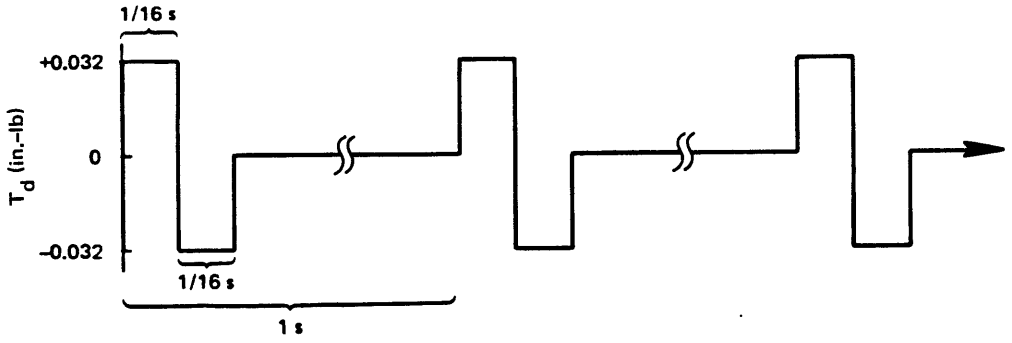

Figure 4-5. Tape drive disturbance.

4.1.2 Low Frequency External Torques

Worst case external torque magnitude is much lower than all internal disturbances, and dominant effects are modeled by

$$T_{db} = [0.0906 + 1.21 \sin \beta] \times 10^{-3} \text{ in.-lb}$$

$$T_{da} = [-0.22 \sin \beta + 0.212 \sin (\beta - 26.6)] \times 10^{-3} \text{ in.-lb}$$

where $\beta = \omega_0 t$ for circular orbits. Body torques are caused by solar pressure and magnetic residuals, while gravity gradient effects act largely on the solar array. Although these torques are comparatively low, since they act over a long period of time and are external, total system momentum can be significantly changed as was seen in Figure 3-4. The addition of an estimator and array drive compensation does not alter the momentum-accumulation in the reaction wheel, nor increase pitch pointing error contribution, which remains under 1 arcsecond as previously illustrated.

The secular accumulation of angular momentum cannot continue indefinitely so to dump excess momentum magnetic torquing coils can be switched on when the satellite is in certain regions of the earth's magnetic field. Since the torque of the coil is known, a bias is introduced into the controller to drive the wheel and ideally not introduce attitude errors. In effect, the control law only has to handle the

transient difference between the coil's torque and the wheel's biased torque, which in worst case is under 0.0004 in.-lb for the pitch axis. The ability to resist torques of this magnitude has already been demonstrated.

4.1.3 Inertial Cross Coupling

Pitch motion is not fully decoupled from the other axes, as was initially assumed. Furthermore, the total spacecraft inertia is not fixed but varies with array position as listed in Table 4-1.

Table 4-1. Flight inertial values (in.-lb-s^2) as function of solar panel angle.

Panel Angle (deg)	0	45	90	135	180	225	270	315
I_X	7973	7539	7233	7538	7973	7539	7233	7539
I_Y	7234	7668	7973	7668	7234	7668	7973	7668
I_Z	1683	1683	1683	1683	1683	1683	1683	1683
I_{XY}	+1.3	-362	+1.3	+365	+1.3	-363	+1.3	+365
I_{XZ}	-803	-786	-758	-729	-713	-729	-758	-786
I_{YZ}	-43	-77	-88	-77	-43	-9	+1.5	-9

Pitch-yaw coupling is quite high for all array positions, although roll motion is nearly decoupled. In the on-orbit case, satellite motion is ideally restricted to a low steady-state pitch rate so cross-coupling effects should not be a difficulty. As a worst case test of stability satellite transient responses to initial errors in each axis were run on a four-degree-of-freedom simulation developed for this satellite at CSDL.

Existing control law gains were used on the yaw and roll axes, while the proposed pitch and array estimator/controller was implemented on the third axis. Figures 4-6 through 4-8 plot each case. Notice that pitch and yaw are quite coupled, and an error in one axis excites the other, while roll motion is almost independent. It is also interesting that the pitch response drives the yaw reaction wheel to nearly twice the level the pitch wheel reaches. The entire loop is stable, and although errors do not remain in their initial axes, all transients decay as fast as a single axis alone.

One approach to solving the cross coupling problem would be to incorporate the motion of all three axes into the model and determine an optimal control law that "knows" the nature of the coupling. No longer a linear problem, a linearized model can be derived for small deviations. Since array position determines much of the coupling, such a linear model would also be time-varying, although cyclic. Whether or not the additional computational burden is better than the performance demonstrated in Figures 4-6, 4-7, and 4-8 is a matter of judgement.

4.2 Summary

Anticipated worst-case pitch and array peak errors for the various disturbances discussed are summarized in Table 4-2.

All of the steady state disturbances are significantly less than the 8.6 arcseconds rms pointing error introduced by star mapper measurement noise. If current gyros were used for sensors, estimation error, as summarized in Table 3-4, is then not the dominant cause of mean-square pointing error.

The results of torque disturbance in Table 4-2 would be a good worst-case representation.

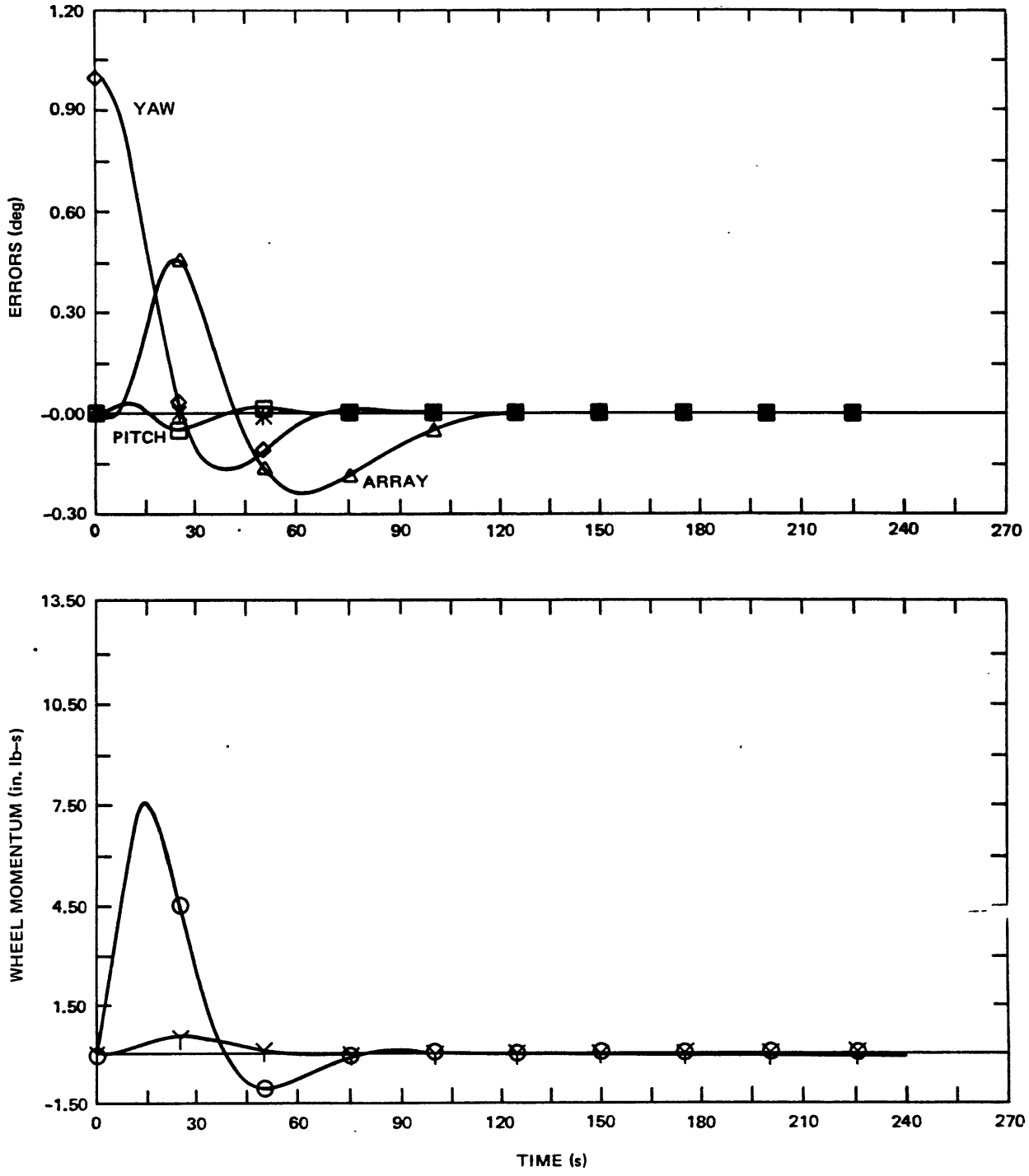

Figure 4-6. 4-DOF rigid body simulation.

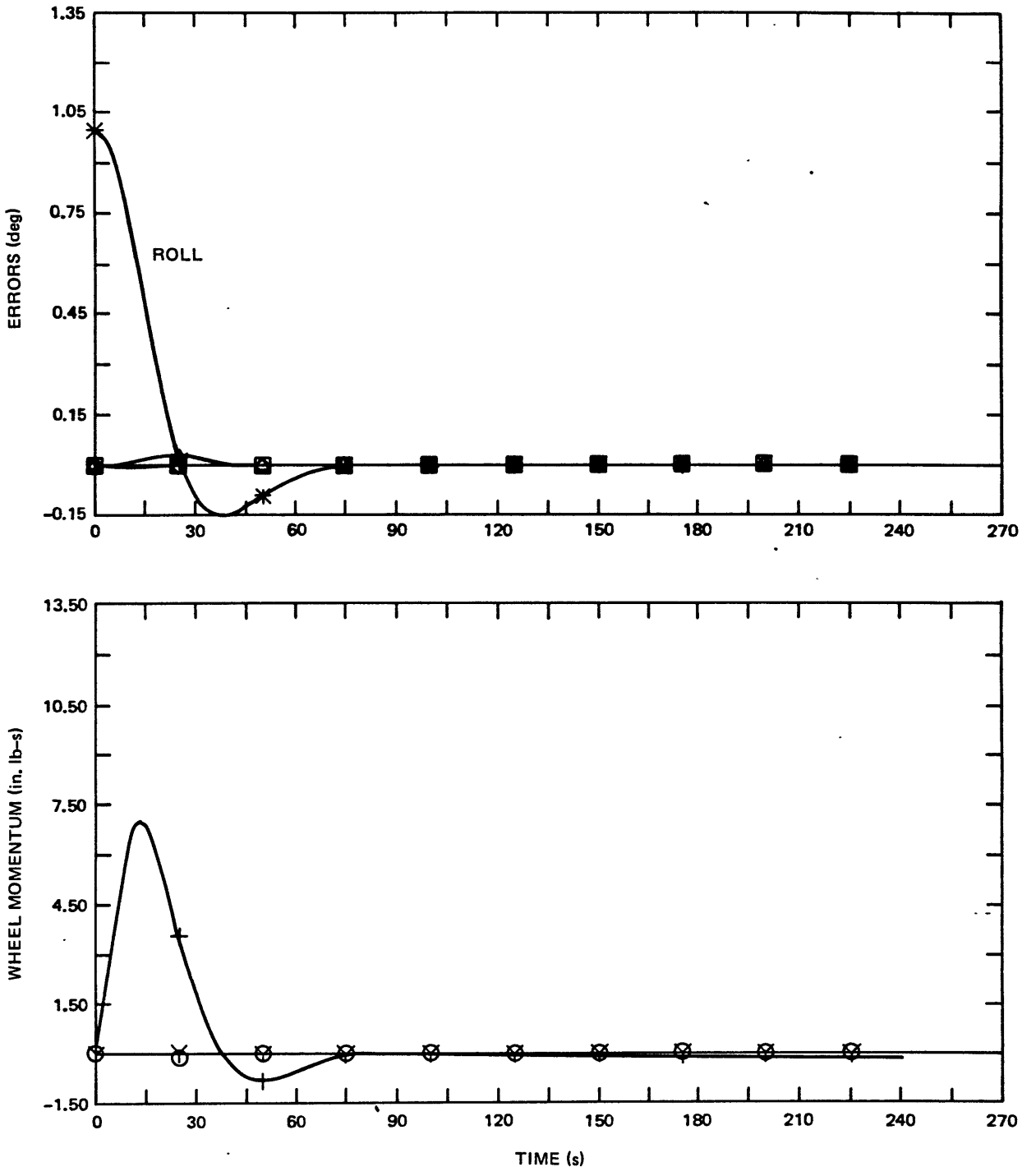

Figure 4-7. 4-DOF rigid body simulation, 2-Hz filter/controller on pitch and array loops.

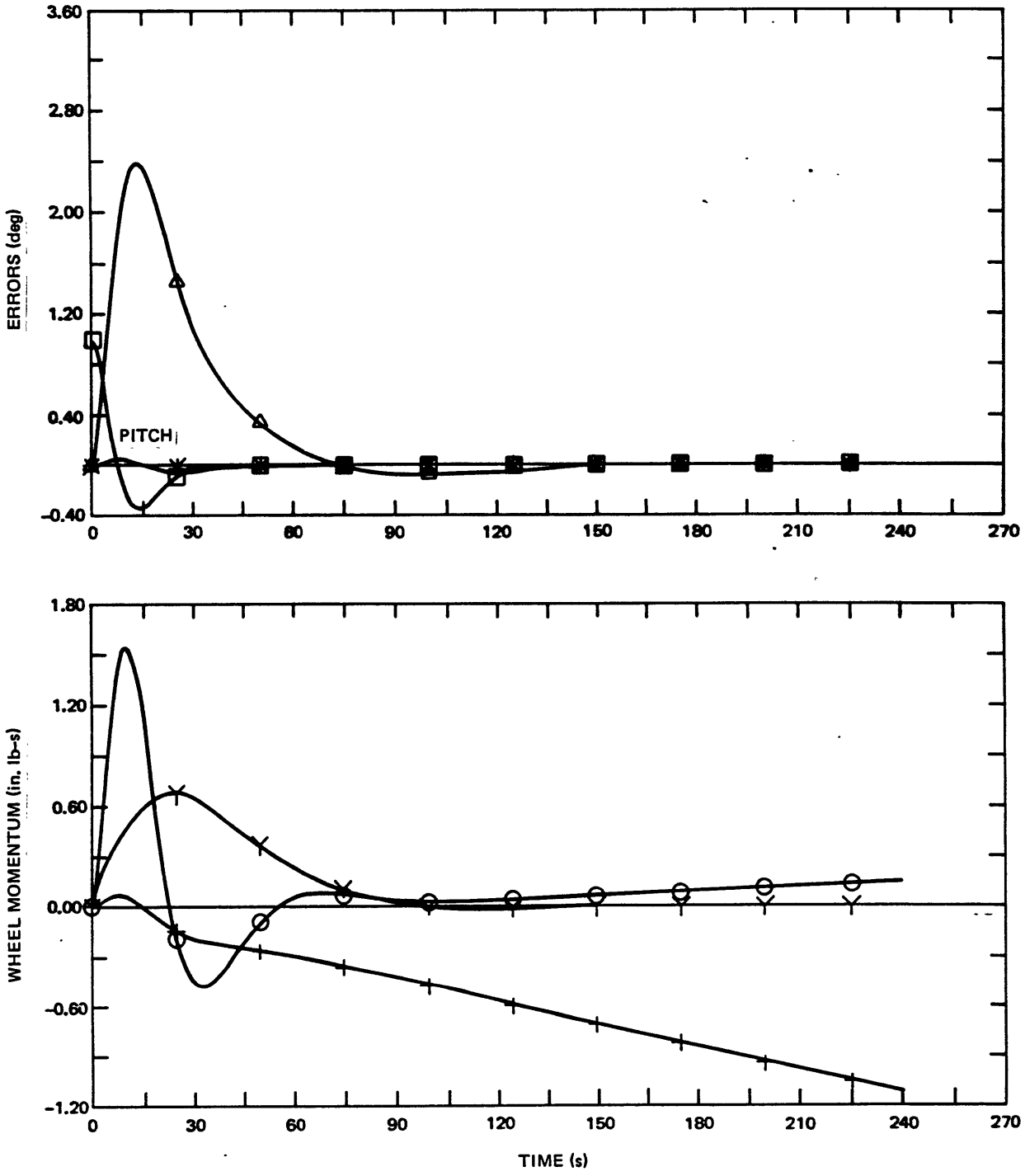

Figure 4-8. 4-DOF rigid body simulation, 2-Hz filter/controller on pitch and array loops.

Table 4-2. Peak pointing errors.

Disturbance	Peak Error	
	Pitch (arcsecond)	Array (degree)
SAD cogging	6	0.18 ± 0.002
6-Hz telescope scanning	0.13	insignificant
RW cogging at 1 r/min	0.036	insignificant
Recorder drive	0.001	insignificant
External torques	0.072	0.05
1° yaw error	166.0	0.46
1° roll error	10.1	0.029

The disturbance model assumed in filter design was a white, Gaussian random sequence of rms 0.73 in.-lb of the body and 1 in.-lb on the solar array. It is interesting to compare the mean-square pointing error predicted for these random disturbances with the results calculated in this section. Closed-loop system covariance, as discussed in Section 3.3, temporarily stabilizes to rms errors of 0.15 degree pitch and 0.2 degree array before rms momentum accumulation exceeds the wheel limit. The disparity in the two results indicates that the white torque noise intensity chosen is a severe model. However, the rationale for choosing the disturbance model involved more than simulating with a white noise a different class of processes. A major consideration in selecting a process intensity was to ensure that estimation errors decayed faster than the control law could follow so, control power would not be expended tracking an erroneous estimate. In this case it may be possible to improve pointing accuracy by reiterating filter design in light of the results derived in this chapter.

Except for the array drive, the proposed controller is capable of dealing effectively with the disturbance environment that the satellite operates in. Although a scheme of controlling array cogging is presented,

if an optimal controller were to be implemented it would be desirable to replace the current motor with a more linear actuator. These results also place a lower bound on attitude estimation accuracy. It does not seem necessary to know attitude as well as rate integrating gyros allow, since internal disturbances become the dominant source of steady state mean-square error. In the worst case, the proposed star mapper can introduce most of the error. Fortunately estimation error can be lowered, if desired, while not much can be done about the disturbance environment.

CHAPTER 5

CONCLUSION

A linear time invariant controller is suitable for on-orbit attitude control of this satellite. The task of the engineer can be reduced to choosing a structure and the associated gains. Classical compensation is a powerful tool for deriving gains, but it does not always offer good hints on structure, particularly for a multi-input, multi-output problem. This thesis shows that LQG optimal control theory directly accomplishes both tasks. In addition, the introduction of an estimator allows rigorous handling of noisy data. The benefit of this approach is an improvement in both deterministic and stochastic performance, while the primary drawback is an increase in required computer operations.

The structural difference between the controllers arrived at via classical theory versus modern theory for the pitch and array loops is illustrated in Figure 5-1. All of the system outside the heavy dashed lines represents satellite dynamics and the current controller, while the feedback paths inside the center block represent those introduced by optimal theory. A number of interesting insights into this problem can be seen. The coupling introduced by the effect of array drive torque on the satellite body and by measuring relative array position is obvious. One of the new cross-feed paths, using gains $[f_{21}, f_{22}, f_{23}]$ bypasses the reaction wheel and commands array drive torque to null body errors. The negative sign of these gains is a result of the torque sign covention, and can also be seen by tracing through the loop.

Another cross-feed path, through gains [f_{14}, f_{15}], commands reaction wheel torque as a function of array error to oppose the disturbance created on the body by the array drive. The effect of these cross feeds is illustrated by the transient responses in Section 3.1. It is possible to arrive at these new feedbacks simply by requiring full state feedback but the problem of selecting gains still remains. By requiring the controller to optimize a quadratic performance index, a unique set of gains results. Of course most of the signal flow in Figure 5-1 is not as direct as indicated. All the quantities transmitted through control gains are the outputs of some form of estimator, which creates the greatest increase in controller complexity.

Full state estimation is not entirely detrimental. A second important advantage of LQG theory is the manner noisy data is used. While knowledge of measurement and disturbance statistics may not be precise, the ability to quantitatively weight good data more than poor data is much more rigorous than treating all outputs as noise-free sources. Frequency domain stochastic techniques are well developed and useful for analyzing the effect of noise on controller design. They do not, however, offer much help with attempting to reduce the effect of noise, unless one wishes to enter the realm of Wiener filtering and compensation. A separate estimator allows the effects of measurement noise to be approached without a specific control law in mind. The framework of linear optimal estimation provides a basis for selecting a set of measurements or determining quality limits as is done for the star map-gyros tradeoff study in Section 3.2.

The issue of complexity needs to be addressed. For this example, satellite attitude error, rate, and integral and array error are determined anyway for the present controller. With those quantities, the on-board computer performs 3 multiplies and 2 adds each 1/2 second for pitch control, while array control is actually implemented by an analog circuit within the motor. If a full state feedback control law is desired for the pitch loop, an array rate and wheel momentum estimate

would also be needed. The extra computation required using portions of the estimator developed in Section 3.2 is 14 multiplies and 11 adds. To calculate the controls, given a state estimate, 12 multiplies and 10 adds for a total computational increase of 23 multiplies and 19 adds, are required. Proportionally this seems to be a major increase. Using arithmetic execution time estimates for the Block 5D computer (RCA 1976), these extra calculations would require at most 2 milliseconds. In normal operation, the computer uses 20.5 milliseconds of the 500 millisecond cycle in the "ACS" mode for attitude control, but not including estimation, processing. By comparison, the computational increase to support an optimal controller is not at all severe.

Performance gained from this increase in complexity was seen in two ways. Deterministically, the new cross feeds allow array drive torque to be a useful control instead of a disturbance. Stochastically, reduced sensitivity to measurement noise was demonstrated in Section 3.3. Although not dramatic improvements, the ability to improve pointing and reduce wheel activity is significant in light of the rigid performance specifications the current controller already meets.

Certain hardware changes, in addition to the sensor options discussed in Section 3.2, would enhance implementation of an optimal controller. The array drive mechanism is a source of particular difficulty. Improving measurement accuracy, perhaps including direct rate estimation, would be profitable. The direct drive nature of the motor could be changed to reduce the cogging effect eliminating the need for local compensation. A smooth linear reduction gear train driven by a faster motor offers an attractive replacement. The current reaction wheel commutation electronics were not designed for frequent low-noise speed monitoring, so the addition of a tachometer may be helpful.

Useful insights into the kinematics of this particular satellite have been gained by a different approach to controller synthesis. By understanding how the two bodies of theory interplay, a control engineer is better able to exploit the strengths of each, and should be able to approach new problems without the artifical limitations imposed by what is mathematically convenient according to one.

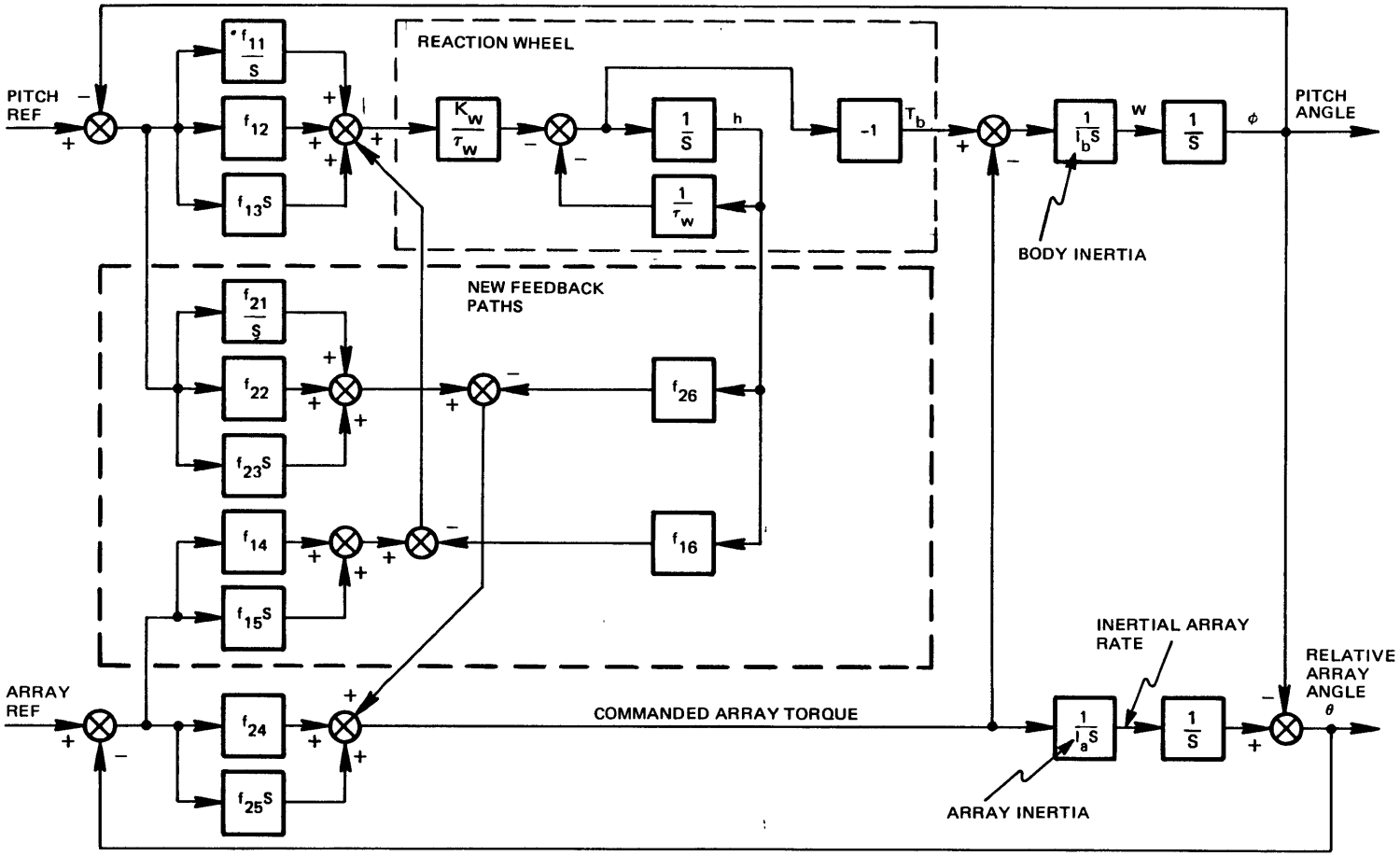

Figure 5-1. Functional block diagram.

APPENDIX A

MODEL DEVELOPMENT

To derive the rotational equations of motion, split the satellite into two bodies at the array drive motor as shown in Figure A-1.

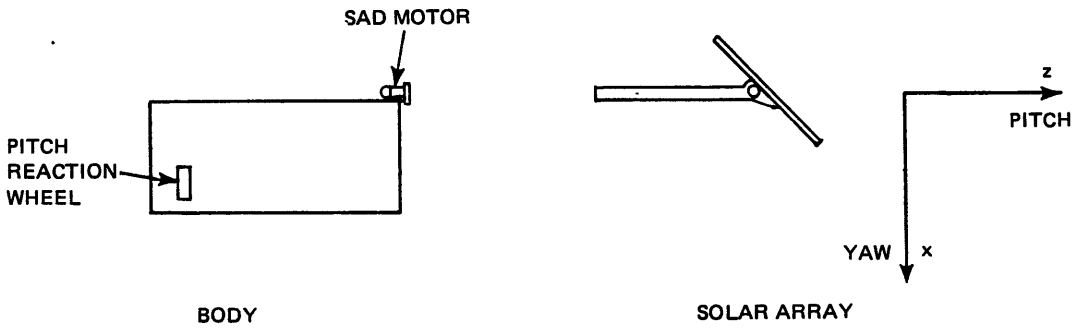

Figure A-1.

Define the parameters:

T_{cb} - Control torque applied to spacecraft body

T_{ca} - Control torque applied to solar array

T_{db} - Disturbance torques acting on body

T_{da} - Disturbance torques acting on array

ϕ - Inertial pitch angle

ω - Inertial pitch rate

θ - Relative solar array angle

I_b - Body moment of inertia about pitch axis

I_a - Array moment of inertia about pitch axis

Figure A-2 illustrates the coordinate convention adopted for the array and body orientations with respect to an inertial reference frame. The view is along the pitch axis.

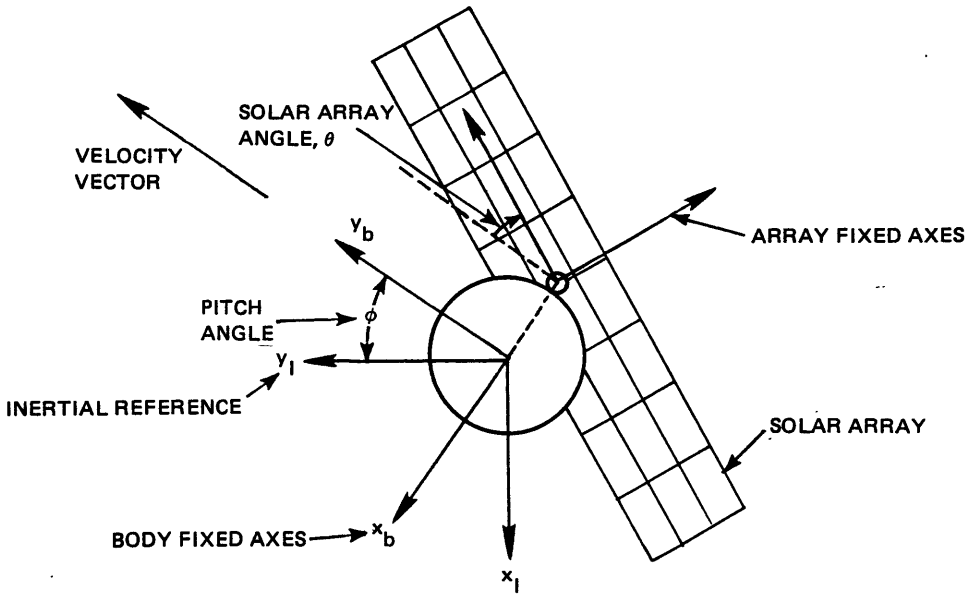

Figure A-2. Coordinate convention.

Writing laws of motion for the array and body separately

$$\sum T_{BODY} = T_{cb} - T_{ca} + T_{db} = I_b \dot{\omega} \qquad \text{(A-1)}$$

$$\sum T_{ARRAY} = T_{ca} + T_{da} = I_a (\dot{\omega} + \ddot{\theta}) \qquad \text{(A-2)}$$

Solve (A-1) for $\dot{\omega}$

$$\dot{\omega} = \frac{1}{I_b} T_{cb} - \frac{1}{I_b} T_{ca} + \frac{1}{I_b} T_{db} \qquad \text{(A-3)}$$

Substitute (A-3) into (A-2)

$$T_{ca} + T_{da} = I_a\left(\frac{1}{I_b} T_{cb} - \frac{1}{I_b} T_{ca} + \frac{1}{I_b} T_{db} + \ddot{\theta}\right) \qquad \text{(A-4)}$$

Solve (A-4) for $\ddot{\theta}$

$$\ddot{\theta} = \left(\frac{1}{I_a} + \frac{1}{I_b}\right) T_{ca} - \frac{1}{I_b} T_{cb} + \frac{1}{I_a} T_{da} - \frac{1}{I_b} T_{db} \qquad \text{(A-5)}$$

Command torque to the satellite body is developed with a reaction wheel that has the following transfer function:

$$\frac{T_{cb}(s)}{V_c(s)} = \frac{K_w s}{\tau_w s + 1} \qquad \begin{aligned} K_w &= 75 \text{ in.-lb-s/V} \\ \tau_w &= 600 \text{ s} \end{aligned} \qquad \text{(A-6)}$$

The long time constant models the buildup of back-emf as the wheel speeds up under a constant demand. For low wheel speeds and over times short in comparison to τ_w the reaction wheel acts as a dc gain of magnitude $K_w/\tau_w = 0.125$ in.-lb/volt to a step command.

Define h(t) to be the momentum of the reaction wheel. The torque applied to the spacecraft is exactly -d/dt h(t), so the transfer function of wheel momentum to command voltage is the integral of Eq. (A-6)

$$\frac{h(s)}{V_c(s)} = \frac{-K_w}{\tau_w s + 1} \qquad \text{(A-7)}$$

Equation (A-7) corresponds to the differential equation:

$$\tau_w \dot{h}(t) + h(t) = -K_w V_c(t)$$

$$\dot{h}(t) = -\frac{1}{\tau_w} h(t) - \frac{K_w}{\tau_w} V_c(t) \qquad \text{(A-8)}$$

Since $T_{cb} = -\dot{h}$, the torque output of the wheel is

$$T_{cb} = \frac{1}{\tau_w} h(t) + \frac{K_w}{\tau_w} V_c(t) \qquad \text{(A-9)}$$

The array drive motor is actually a very nonlinear device with coloumb friction and prominant cogging effects. However, it will be modeled as a pure torque transducer and T_{ca} considered a controllable input. Implementation issues of this assumption are discussed elsewhere.

Substituting (A-9) into (A-3) and (A-5)

$$\dot{\omega} = \frac{1}{I_b}\left(\frac{1}{\tau_w} h + \frac{K_w}{\tau_w} V_c\right) - \frac{1}{I_b} T_{ca} + \frac{1}{I_b} T_{db}$$

$$\dot{\omega} = \frac{1}{I_b \tau_w h} + \frac{K_w}{I_b \tau_w} V_c - \frac{1}{I_b} T_{ca} + \frac{1}{I_b} T_{db}$$

$$\ddot{\theta} = \left(\frac{1}{I_a} + \frac{1}{I_b}\right) T_{ca} - \frac{1}{I_b}\left(\frac{1}{\tau_w} h + \frac{K_w}{\tau_w} V_c\right) + \frac{1}{I_a} T_{da} - \frac{1}{I_b} T_{db} \qquad \text{(A-10)}$$

$$\ddot{\theta} = -\frac{1}{I_b \tau_w} h - \frac{K_w}{I_b \tau_w} V_c + \left(\frac{1}{I_a} + \frac{1}{I_b}\right) T_{ca} - \frac{1}{I_b} T_{db} + \frac{1}{I_a} T_{da} \qquad \text{(A-11)}$$

Define q to be the integral of attitude

$$q(t) = \int_0^t \phi(t)\, dt$$

so

$$\dot{q} = \phi \qquad \text{(A-12)}$$

"q" will provide a state variable that can be fed back to implement integral compensation, which is necessary to null out the effects of near steady-state disturbance torques.

Define the state vector

$$\underline{\dot{x}} = [q \quad \phi \quad \omega \quad \theta \quad \dot{\theta} \quad h]^T$$

Equations (A-8), (A-10), (A-11), and (A-12) are a set of state differential equations, which can be written in the familiar form

$$\underline{\dot{x}} = A\underline{x} + B\underline{u} + G\underline{w} \qquad \text{(A-13)}$$

where the control vector $\underline{u}$ is defined

$$\underline{u} = \begin{bmatrix} V_c(t) \\ \\ T_{ca}(t) \end{bmatrix}$$

and the disturbance vector $\underline{w}$ is defined

$$\underline{w} = \begin{bmatrix} T_{db} \\ \\ T_{da} \end{bmatrix}$$

The matrices A, B, and G are defined as follows:

$$A = \begin{bmatrix} 0 & 1 & 0 & 0 & 0 & 0 \\ 0 & 0 & 1 & 0 & 0 & 0 \\ 0 & 0 & 0 & 0 & 0 & 1/I_b\tau_w \\ 0 & 0 & 0 & 0 & 1 & 0 \\ 0 & 0 & 0 & 0 & 0 & -1/I_b\tau_w \\ 0 & 0 & 0 & 0 & 0 & -1/\tau_w \end{bmatrix}$$

$$B = \begin{bmatrix} 0 & 0 \\ 0 & 0 \\ \frac{K_w}{I_b\tau_w} & \frac{-1}{I_b} \\ 0 & 0 \\ \frac{-K_w}{I_b\tau_w} & \left(\frac{1}{I_a} + \frac{1}{I_b}\right) \\ \frac{-K_w}{\tau_w} & 0 \end{bmatrix} \qquad G = \begin{bmatrix} 0 & 0 \\ 0 & 0 \\ 1/I_b & 0 \\ 0 & 0 \\ -1/I_b & 1/I_a \\ 0 & 0 \end{bmatrix}$$

Numerical values of the model parameters are:

$$I_a = 877 \text{ in.-lb-s}^2$$

$$I_b = 891 \text{ in.-lb-s}^2$$

$$K_w = 75 \text{ in.-lb-s/V}$$

$$\tau_w = 600 \text{ s}$$

Since the control law is to be implemented in a digital computer sampling at a rate of 2 Hz, a set of difference equations that models the pitch dynamics only at the sample times may be used instead of the differential equations represented by (A-13). If the control input is held constant between sample intevals, and the disturbance input varies slowly enough that a piecewise constant function is an accurate approximation, the model may be written as

$$\underline{x}_{i+1} = \Phi\underline{x}_i + \Lambda\underline{u}_i + \Gamma\underline{w}_i \tag{A-14}$$

$$t_{i+1} - t_i = 0.5 \text{ s}$$

The state transition matrix, Φ, the control effectiveness matrix, Λ, and the disturbance weighting matrix, Γ, are given by

$$\Phi = \exp [AT] \tag{A-15}$$

$$\Lambda = \int_0^T \Phi(T - \tau)B \, d\tau \tag{A-16}$$

$$\Gamma = \int_0^T \Phi(T - \tau)G \, d\tau \tag{A-17}$$

$$T = 0.5 \text{ s}$$

Evaluating A-15, A-16, and A-17 with a control theory software package developed at the Charles Stark Draper Laboratory, numerical values are:

$$\Phi = \begin{bmatrix} 1 & 0.5 & 0.125 & 0 & 0 & 3.8962 \times 10^{-8} \\ 0 & 1 & 0.5 & 0 & 0 & 2.3375 \times 10^{-7} \\ 0 & 0 & 1 & 0 & 0 & 9.3489 \times 10^{-7} \\ 0 & 0 & 0 & 1 & 0.5 & -2.3375 \times 10^{-7} \\ 0 & 0 & 0 & 0 & 1 & -9.3489 \times 10^{-7} \\ 0 & 0 & 0 & 0 & 0 & 9.9917 \times 10^{-7} \end{bmatrix}$$

$$\Lambda = \begin{bmatrix} 2.9221 \times 10^{-6} & -2.3382 \times 10^{-5} \\ 1.7532 \times 10^{-5} & -1.4029 \times 10^{-4} \\ 7.0117 \times 10^{-5} & -5.6117 \times 10^{-4} \\ -1.7532 \times 10^{-5} & 2.8282 \times 10^{-4} \\ -7.0117 \times 10^{-5} & 1.1313 \times 10^{-3} \\ -6.2474 \times 10^{-2} & 0 \end{bmatrix}$$

$$\Gamma = \begin{bmatrix} 2.3382 \times 10^{-5} & 0 \\ 1.4029 \times 10^{-4} & 0 \\ 5.6117 \times 10^{-4} & 0 \\ -1.4029 \times 10^{-4} & 1.4253 \times 10^{-4} \\ -5.6117 \times 10^{-4} & 5.7012 \times 10^{-4} \\ 0 & 0 \end{bmatrix}$$

APPENDIX B

DERIVATION OF OPTIMAL GAIN RECURSION

Given the linear discrete time system

$$\underline{x}_{i+1} = \Phi \underline{x}_i + B\underline{u}_i$$

and the quadradic cost function $c(\underline{x}, \underline{u})$

$$c = \sum_{i=0}^{L-1} \left(\underline{x}_i^T Q_{xx} \underline{x}_i + \underline{u}_i^T R_{uu} \underline{u}_i \right) + \underline{x}_L^T P_L \underline{x}_L \qquad \text{(B-1)}$$

The control $\underline{u}_i$ that minimizes c is of the form

$$\underline{u}_i = -F_i \underline{x}_i$$

where F_i, the feedback gain matrix is found from the following backwards recursion from i = L to i = 0

$$F_i = \left[B_i^T P_{i+1} B_i + R_{uu} \right]^{-1} B_i^T P_{i+1} \Phi \qquad \text{(B-2)}$$

$$P_i = [\Phi - B_i F_i]^T P_{i+1} [\Phi - B_i F_i] + Q_{xx} + F_i^T R_{uu} F_i \qquad \text{(B-3)}$$

Proof:

Define the minimum cost to complete function at interval i to be the result of applying the optimal sequence of controls, $u_i, \ldots, u_L$ such that the quadradic cost, c, incurred from time i to final time L is minimum.

$$c^o(x_i, i) = \min_{u_i, \ldots, u_L} \sum_{j=i}^{L-1} \left[\underline{x}_j^T Q_{xx} \underline{x}_j + \underline{u}_j^T R_{uu} \underline{u}_j \right] + \underline{x}_L^T P_L \underline{x}_L \qquad \text{(B-4)}$$

When i = L, the cost-to-complete is not dependent on $\underline{u}$, and is given by

$$c^o(x_L) = \underline{x}_L^T P_L \underline{x}_L$$

The solution by dynamic programming asserts that given that the cost to complete is minimum from i+1 to L, the optimal control at i is not a function of the later controls, $\underline{u}_{i+1}, \ldots, \underline{u}_L$, but is that which minimizes only the additional cost incurred by transitioning from $\underline{x}_i$ to $\underline{x}_{i+1}$

$$c^o(\underline{x}_i, i) = \min_{u_i} \left[\underline{x}_i^T Q_{xx} \underline{x}_i + \underline{u}_i^T R_{uu} \underline{u}_i \right] + c^o(\underline{x}_{i+1}, i+1) \qquad \text{(B-5)}$$

Suppose the optimal control sequence $u^o_{i+1}, \ldots, u^o_{L-1}$ is known that produces $c^o(\underline{x}_{i+1}, i)$. Note that $c^o(\underline{x}_{i+1}, i)$ is not entirely determined by $\underline{u}_{i+1}, \ldots, u^o_{L-1}$ since x_{i+1} is a function u_i, $x_{i+1} = \Phi x_i + B u_i$, but $c^o(x_{i+1}, i+1)$ is the lowest possible value that controlling from i+1 to L-1 can produce.

Starting at i = L

$$c^o(x_L, L) = \underline{x}_L^T P_L \underline{x}_L$$

c^o is always of the form

$$c^o(x_i, i) = \underline{x}_i^T P_i \underline{x}_i$$

The optimal control, u_{L-1}, is found by substituting $c^o(x_L, L)$ into Eq. (B-5), and searching over all possible controls to find the one that minimizes $c(x_{L-1}, L-1)$

$$c^o(x_{L-1}, L-1) = \underline{x}_{L-1}^T P_{L-1} \underline{x}_{L-1} = \min_{u_{L-1}} [\underline{x}_{L-1}^T Q_{xx} \underline{x}_{L-1} + \underline{u}_{L-1}^T R_{uu} \underline{u}_{L-1})$$

$$+ (\Phi \underline{x}_{L-1} + B\underline{u}_{L-1})^T P_L (\Phi \underline{x}_{L-1} + B\underline{u}_{L-1}) \qquad \text{(B-6)}$$

To minimize $\underline{x}_{L-1}^T P_{L-1} \underline{x}_{L-1}$, differentiate with respect to $\underline{u}_{L-1}$, and set the result to zero

$$0 = \frac{d}{du_{L-1}} (\underline{x}_{L-1}^T P_{L-1} \underline{x}_{L-1}) = 2R_{uu}\underline{u}_{L-1} + 2B^T P_L (\Phi \underline{x}_{L-1} + B\underline{u}_{L-1})$$

Collecting terms of $\underline{x}_{L-1}$ and $\underline{u}_{L-1}$

$$[B^T P_L B + R_{uu}]\underline{u}_{L-1} = -B^T P_L \Phi \underline{x}_{L-1}$$

If R_{uu} is specified positive definite, and P_L positive semi-definite, $\underline{u}_{L-1}$ can be solved for

$$\underline{u}_{L-1} = -[B^T P_L B + R_{uu}]^{-1} B^T P_L \Phi \underline{x}_{L-1} \qquad \text{(B-7)}$$

and P_{L-1} must now be solved for.

Define

$$F_{L-1} = [B^T P_L B + R_{uu}]^{-1} B^T P_L$$

so

$$\underline{u}_{L-1} = -F_{L-1}\underline{x}_{L-1} \tag{B-8}$$

Substituting (B-8) into (B-6), dropping the L-1 subscript on $\underline{x}$ and $\underline{u}$

$$\underline{x}^T P_{L-1}\underline{x} = \underline{x}^T Q_{xx}\underline{x} + \underline{x}^T F^T R_{uu} F\underline{x} + \underline{x}^T(\Phi - BF)^T P_L(\Phi - BF)\underline{x}$$

All forms are quadradic in $\underline{x}$, so for equality

$$P_{L-1} = Q_{xx} + F^T R_{uu} F + (\Phi - BF)^T P_L(\Phi - BF)$$

which is Eq. (B-3) for i = L-1. The control u_{L-2} is solved with the same approach, and the recursion for F_i and P_i propagated backwards until i = 0.

This approach to the optimal controller was developed by Widnall (1968), and differs from the original solution by Kalman and Kopke (1958) in that $\underline{u}_i$ is a vector, and P_i is symmetric.

APPENDIX C

SAD COMPENSATION

The array drive motor currently used on the satellite is a 96 pole direct drive motor, which nominally rotates exactly once per orbit.

Two undesirable nonlinear effects, couloumb friction and cogging, disallow the use of a linear model for control synthesis. The output torque of the motor is modeled as

$$T_{ca} = K_T(V_a - K_b\dot{\theta}) + \underbrace{0.18 \sin(96\theta)}_{\text{Cogging Torque}} - \underbrace{1.25\,|\dot{\theta}|/\dot{\theta}}_{\substack{\text{Couloumb} \\ \text{Friction}}} \text{ in.-lb} \qquad \text{(C-1)}$$

where

K_T = 0.138 in.-lb/V

K_b = 1.03 V-s/rad

θ = solar array angle (rad)

$\dot{\theta}$ = solar array rate (rad/s)

V_a = motor voltage

As can be seen from the magnitudes of the cogging and friction torques, for on-orbit array control these effects become the primary disturbances the loop must counter.

It is desirable that the SAD motor act as a pure torque transducer. If this is the case, then the array rate will be described by the following differential equation derived in Appendix A.

$$\ddot{\theta} = \frac{1}{I_b \tau_w} h - \frac{K_w}{I_b \tau_w} V_c + \left(\frac{1}{I_a} + \frac{1}{I_b}\right) T_{ca} \qquad \text{(C-2)}$$

where

h = reaction wheel momentum

V_c = wheel command voltage

T_{ca} = array command torque

I_a = moment of inertia of array

I_b = moment of inertia of body

K_w, τ_w = reaction wheel parameters

Ogata (1970) points out that a useful approach to controlling nonlinear systems is model-following. If the array were to match the dynamics predicted in Eq. (C-2), then the motor could be considered a pure torque producer. Once integrated, Eq. (C-2) produces an array-rate time function that can be generated by quantities known to the controller

$$\dot{\theta}_r(t) = \int_0^t \left[\frac{-1}{I_b \tau_w} h(t) - \frac{K_w}{I_b \tau_w} V_c(t) + \left(\frac{1}{I_a} + \frac{1}{I_b}\right) T_{ca}(t)\right] dt \qquad \text{(C-3)}$$

Since the controller issues commands only at discrete time points, the actual reference signal will be a continuous series of ramp functions, without any jump discontinuities.

The proposed local compensation for the SAD motor is diagrammed in Figure C-1.

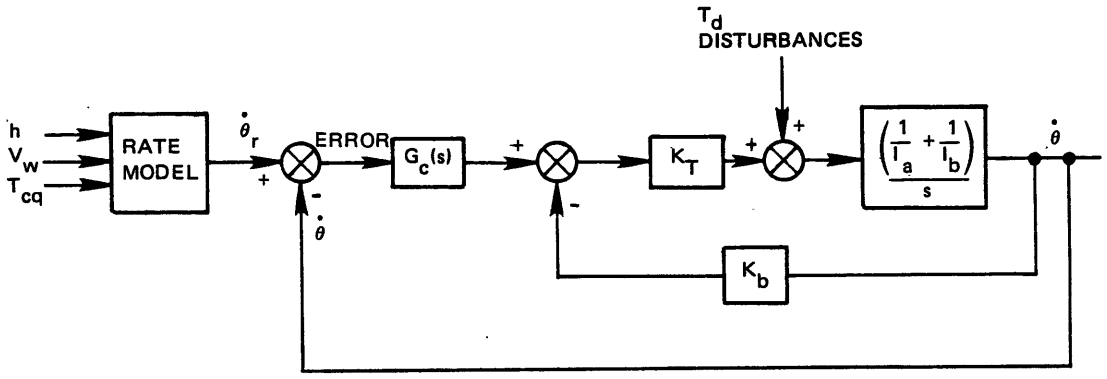

Figure C-1. SAD local compensation.

The compensator $G_c(s)$ should satisfy several conflicting objectives. Since the nominal on-orbit array rate is a relatively constant 0.06 °/s, the cogging torque appears at a frequency of 0.1 rad/s. The array loop should have high gain at this frequency to minimize the effects of cogging torque. However, it is not desirable that the SAD compensator be sensitive to orbit rate disturbances. One of the attractive features of optimal control of the pitch loop is the use of the solar array to absorb some cyclic momentum. A rigid local compensator would not allow the array to wander and would pass all external disturbances to the reaction wheel. Finally, the response time of the loop needs to be short compared to the 0.5 s sampling rate in order not to invalidate the overall discrete time model assumed for the combined pitch and array loops. Satisfying the first and last objectives is done with a high gain, however the second objective is best satisfied with a slight negative gain to null out the rate damping term. A sophisticated frequency selective compensator is not practical, so the second objective will be met as well as possible with a low order compensator while not compromising the first and third goals.

Ignoring the small viscous damping term, K_b, the open loop transfer function is

$$G_{OL}(s) = \frac{1}{s} G_c(s) K_T \left(\frac{1}{I_a} + \frac{1}{I_b} \right) \qquad \text{(C-3)}$$

and the transmission from disturbance torque to array angle is

$$\frac{\theta(s)}{T_d(s)} = \frac{\frac{1}{s^2}\left(\frac{1}{I_a} + \frac{1}{I_b} \right)}{1 + G_{OL}(s)} \qquad \text{(C-4)}$$

Setting a limit of $|\theta_{max}| = 0.01°$ on the response to cogging torque, the necessary loop gain can be calculated and is found to be 47 dB. The principle external torque the array responds to is caused by gravity gradient effects, and is nominally modeled by

$$T_G(t) = [0.0912 + 1.21 \sin (2\omega_o t)] \times 10^{-3} \text{ in.-lb} \qquad \text{(C-5)}$$

where

ω_o = Orbit rate = 0.06 °/s

If the array is to be free to respond to gravity gradient torques, the open-loop gain must be less than is necessary to suppress the cogging response. Listed in the table below are the maximum open-loop gains allowable for several array deviation limits.

Table C-1. Open-loop gain limits.

Array Response to Gravity Gradient	$\lvert G_{OL}(j\omega) \rvert$
0.1°	51 dB
1°	31 dB
5°	17 dB

Figure C-2 plots the uncompensated ($G_c(s) = 1.0$) open-loop frequency response and illustrates the gain requirements discussed for cogging and external torque response.

A double lead compensator will very nearly fit the open-loop gain requirements, with a lower dc gain than would be required for gain only compensation. The proposed compensator transfer function is

$$G_c(s) = \frac{K_c \left(\frac{1}{\tau_1} s + 1\right)^2}{\left(\frac{1}{\tau_2} s + 1\right)^2}$$

where

$\tau_1 = 500$ s

$\tau_2 = 10$ s

$K_c = 56.2$

Figure C-3 illustrates the compensated open-loop frequency response. Loop stability is assured with an infinite gain margin and a 90° phase margin.

Closed-loop transmission of disturbance torques to array angle as shown in Figure C-4. At cogging frequency, the attenuation is -60 dB which will result in a peak deflection of 0.0103 degrees. At twice orbit rate, gravity gradient torque will cause a peak array deflection of 0.78 degree, which still allows some momentum storage in the array.

Although step inputs will not be applied to the SAD loop, response to such an input illustrates the speed of the loop, and is a useful evaluation. In this particular case, the motor torque response to a step commanded torque is exactly proportional to the rate response to a step rate command. Torque is proportional to the derivative of rate and a commanded rate is the integral of a commanded step torque, the integration and differentiation cancel as is shown in Figure C-5.

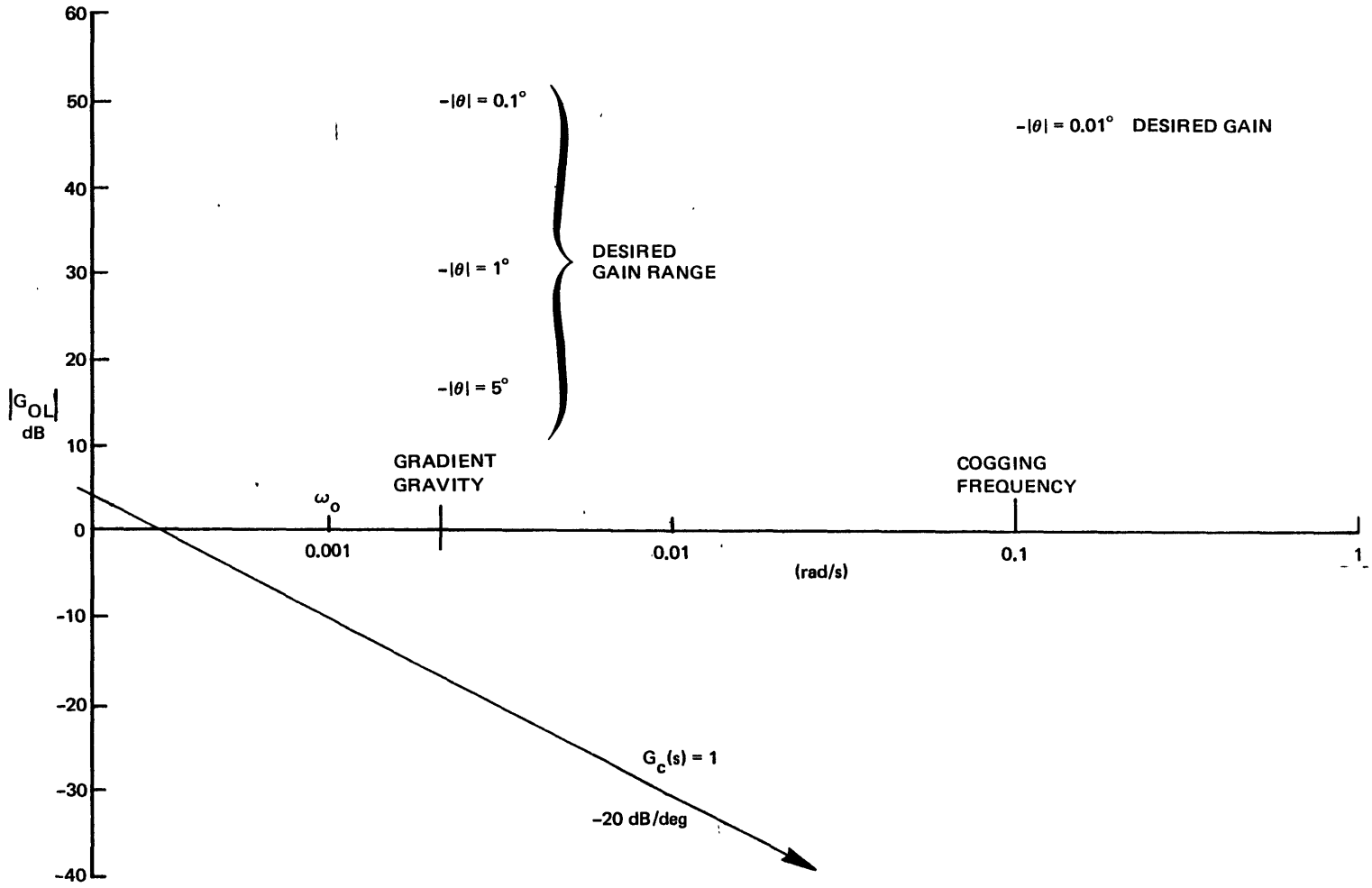

Figure C-2. Open-loop frequency response.

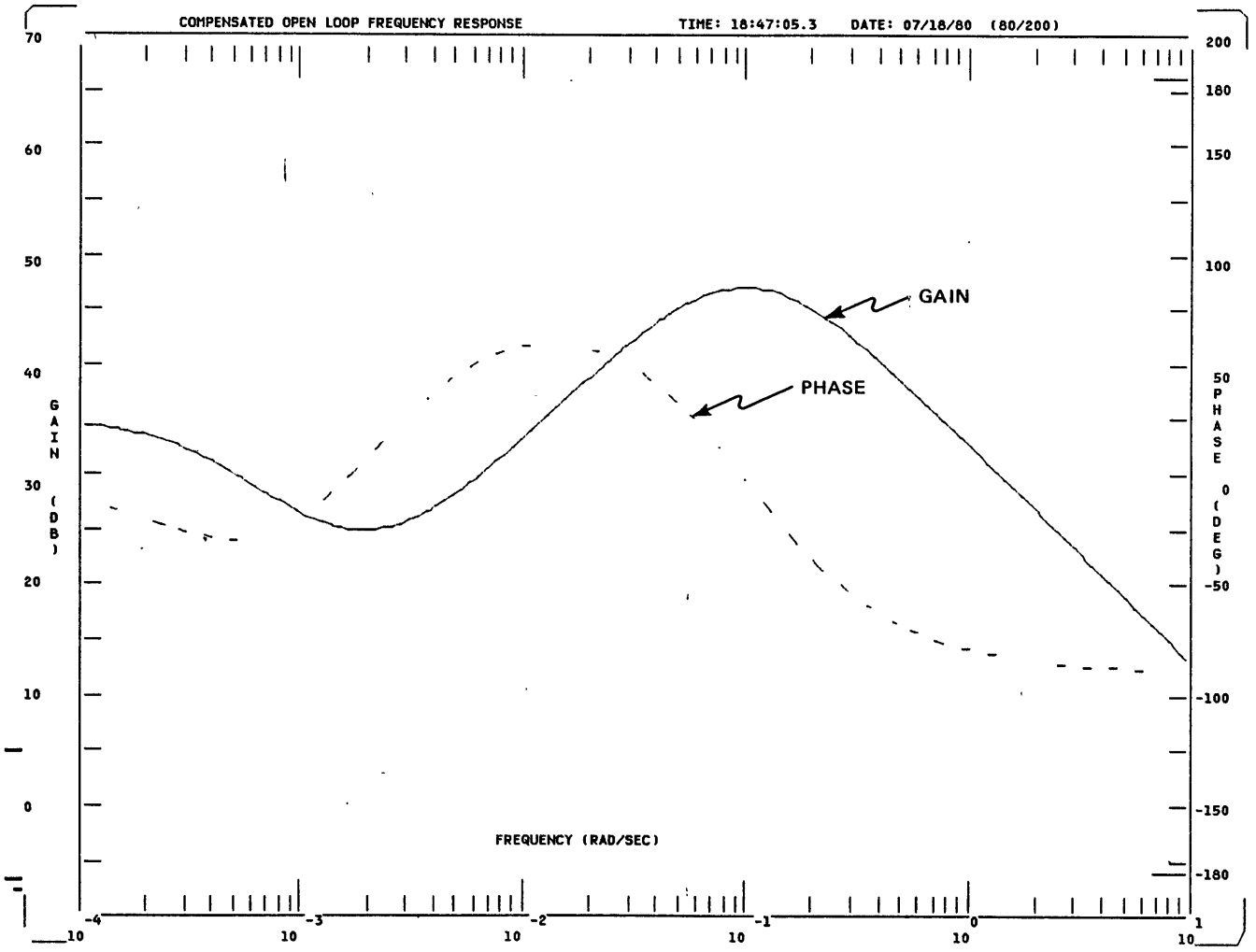

Figure C-3. Compensated open-loop frequency response.

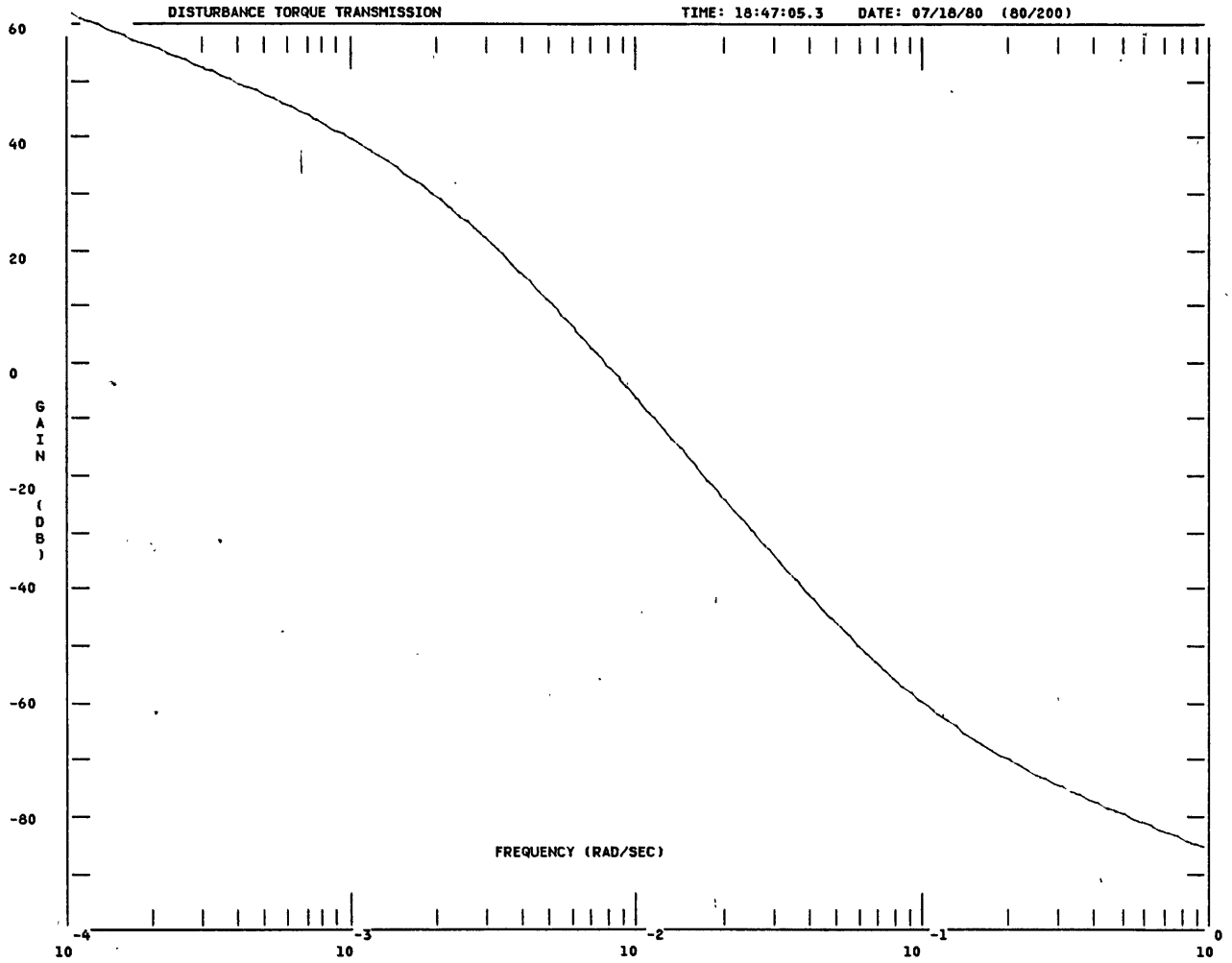

Figure C-4. Disturbance torque transmission.

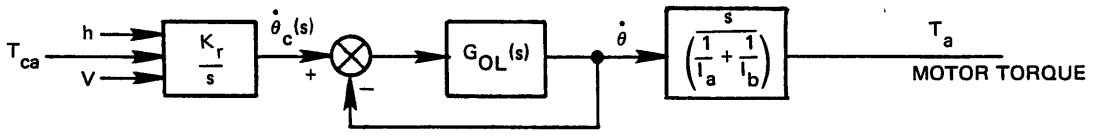

Figure C-5. Closed-loop torque response.

$$\frac{\dot{\theta}(s)}{\dot{\theta}_c(s)} = \frac{G_{OL}(s)}{1 + G_{OL}(s)}$$

$$\frac{T_a(s)}{T_{ca}(s)} = \frac{K_r}{s} \frac{G_{OL}(s)}{1 + G_{OL}(s)} \frac{s}{\left(\frac{1}{I_a} + \frac{1}{I_b}\right)}$$

$$= \frac{K_r}{\left(\frac{1}{I_a} + \frac{1}{I_b}\right)} \frac{\dot{\theta}(s)}{\dot{\theta}_c(s)} \qquad \text{(C-7)}$$

In closed loop, the rate to rate command transfer function is

$$\frac{\dot{\theta}(s)}{\dot{\theta}_c(s)} = \frac{44.491(s + 0.002)^2}{(s + 0.00144)(s + 0.00277)(s + 44.69)} \qquad \text{(C-8)}$$

With a time response to step input of $\theta_c(s) = \frac{1}{s}$

$$\dot{\theta}(t) = 1 - 0.1636e^{-0.00144t} + 0.1592e^{-0.00277t} - 0.9956e^{-44.69t} \qquad \text{(C-9)}$$

A plot of $\dot{\theta}(t)$ to a unit step input for one sample interval is shown in Figure C-6.

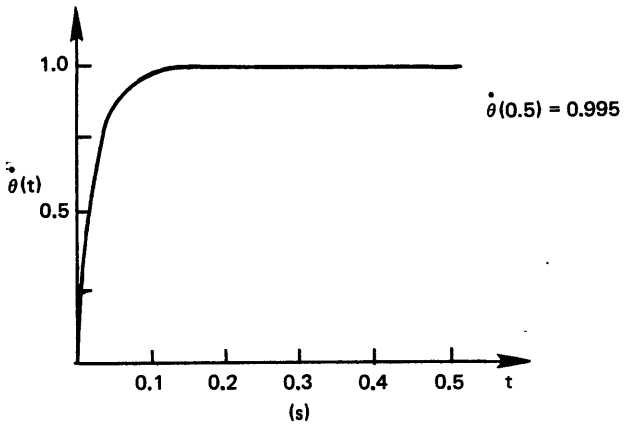

Figure C-6. Rate-step response.

A short response time with respect to the 0.5 s sample time means that the optimal controller will "see" the SAD motor as an almost perfect torque transducer. A final evaluation is to compare two pitch-loop responses under optimal control. The first response, Figures C-7a, b, plot the results of the ideal model. The second simulation incorporated the SAD motor modeled by Eq. (C-1) with the proposed rate compensator and the driving model of Eq. (C-2). Figures C-8 a and b show this response, which differs only slightly from the ideal response. Note the effect of coloumb friction as array rate goes through zero and that the array is now driven to the nominal rate of 0.6 deg/sec.

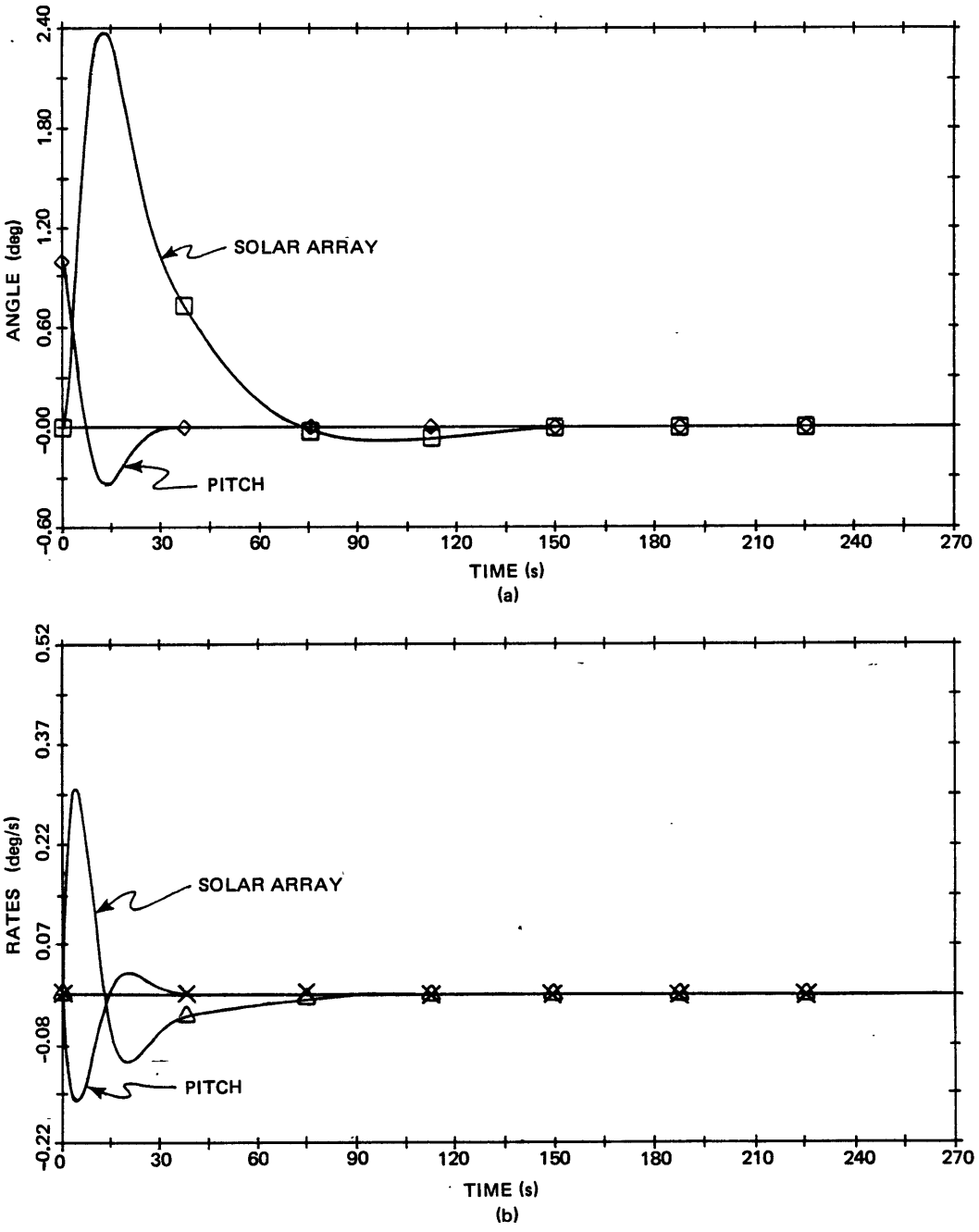

Figure C-7. Deterministic optimal control.

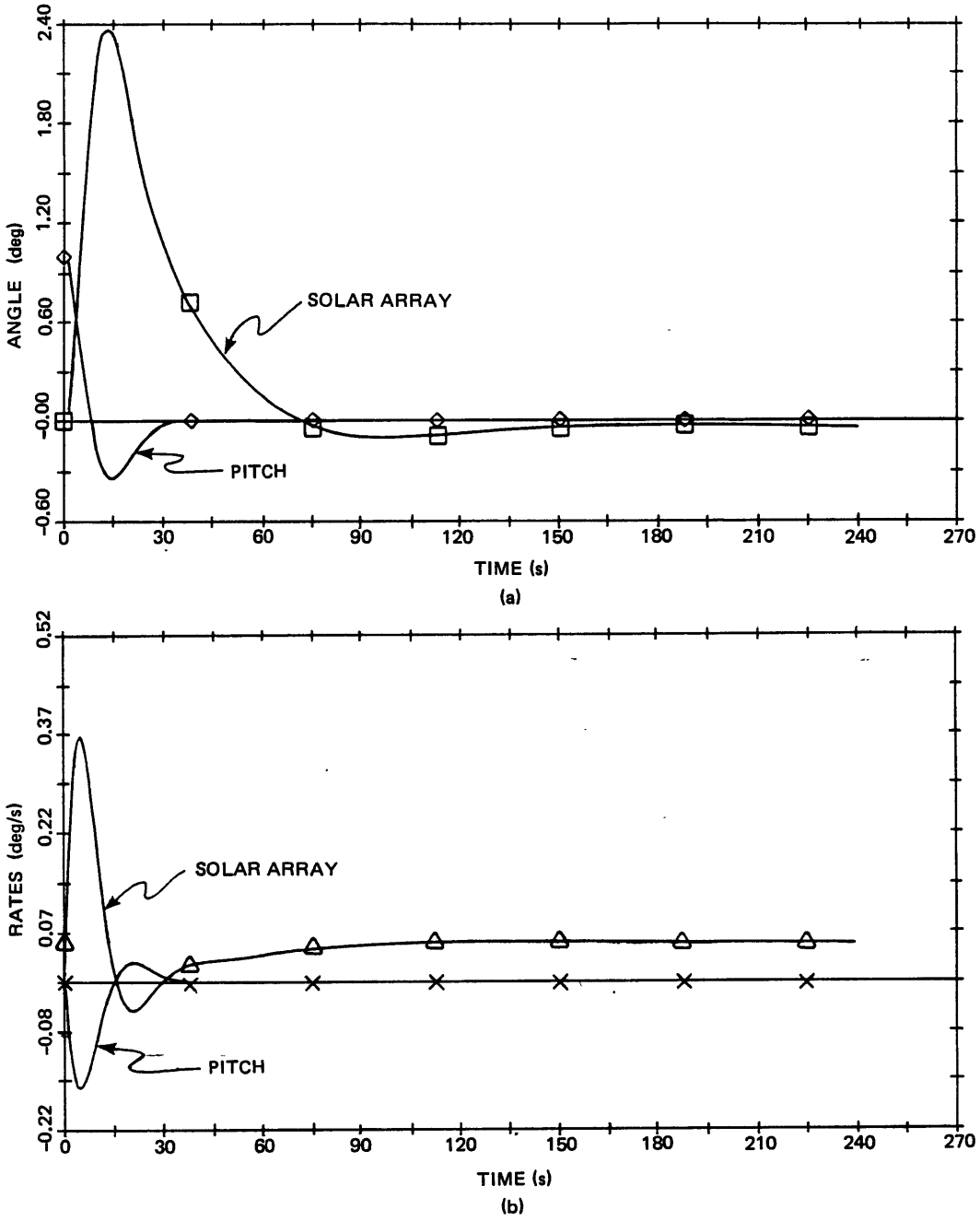

Figure C-8. Optimal control with SAD nonlinearities and compensation.

LIST OF REFERENCES

Bryson, A. E., and Y. C. Ho (1969), Applied Optimal Control, Ginn and Company, Waltham, MA.

Gai, E., J. Harrison, L. Lemos, and K. Daly, (Jan. 1980) "Satellite Navigation and Guidance Performance Analysis", CSDL Report R-1341, Cambridge, MA.

Gelb, A., (1974) Applied Optimal Estimation, MIT Press, Cambridge, MA.

Gray, C. R., and D. G. Youmans, (1979), A CCD Star Mapper Study, Charles Stark Draper Laboratory Report C-5262, Cambridge, MA.

Jazwinski, A. H. (1970), Stochastic Processes and Filtering Theory, Academic Press, New York.

Joseph, P. D., and J. T. Tou (September 1961), "On Linear Control Theory", AIEE Transactions, Applications and Industry, Vol. 80, pp. 193-196.

Kalman, R. E., and R. W. Koepcke, (Nov. 1958) "Optimal Synthesis of Linear Sampling Control Systems Using Generalized Performance Indexes", Trans. ASME, Vol. 80. pp. 1820-1826.

Kalman, R. E. (March 1960), "A New Approach to Linear Filtering and Prediction Problems", Trans. ASME, Series D, Jour. of Basic Eng., Vol. 82, pp. 35-45.

Laning, J. H., and R. H. Battin, (1956), Random Processes in Automatic Control, McGraw-Hill, Inc., New York.

Ozata, K. (1970), Modern Control Engineering, Prentice-Hall, Inc., Englewood Cliffs, N.J.

Pistner, J. S., G. T. Tseng, and L. Muhlfelder, (Oct. 1975), "Multiloop Analysis of a Precision Pointing Spacecraft With Controlled Flexible Appendages", Journal of Spacecraft and Rockets, Vol. 12. pp. 586-591.

RCA Astro Electronics Division (1976), Systems Analysis Report, Vol. 4: "Attitude Determination and Control" and Vol. 6, "Software", RCA, Princeton, N.J.

Truncale, A., W. Koenigsberg, and R. Harris, (February 1972) "Spectral Density Measurements of Gyro Noise", CSDL Report E-2641, Cambridge, MA.

Tseng, G. T., and T. G. Tracy (June 1977), "Application of Quadratic Cost Optimal Control Theory to a Complex Flexible Spacecraft," Dynamics and Control of Large Flexible Spacecraft, (Proceedings of a Symposium held in Blacksburg, VA), L. Meirovitch, ed. pp. 27-40. AIAA.

Widnall, W. S. (1968) Applications of Optimal Control Theory to Computer Controller Design, MIT Press, Cambridge, MA.